Dynamical behavior of microemulsion and sponge phases in thermal equilibrium

M. Hennes [1,2] and G. Gompper [2,1]
[1] *Sektion Physik der Ludwig-Maximilians-Universität München, Theresienstrasse 37, D-80333 München, Germany*
[2] *Max-Planck-Institut für Kolloid- und Grenzflächenforschung, Kantstrasse 55, D-14513 Teltow-Seehof, Germany*
(Received 10 November 1995; revised manuscript received 8 March 1996)

The dynamical behavior of microemulsion and sponge phases is studied with a time-dependent Ginzburg-Landau model. The model has been shown previously to capture many of the essential static properties of these systems. Using a field-theoretic perturbation theory, we calculate the frequency-dependent (complex) viscosity $\eta(\omega)$, sound velocity $c(\omega)$ and damping $D(\omega)$, and the scattering intensity $S(\mathbf{k},t)$ in bulk and film contrast. The viscosity is almost frequency independent for small ω, then drops sharply at a characteristic frequency ω^*, corresponding to a characteristic relaxation time $\tau \sim 1/\omega^*$. The same relaxation time is also found to dominate the sound velocity and damping. The characteristic frequency has the scaling form $\omega^* \sim \xi^{-6}\Omega(q\xi)$, where ξ is the correlation length and q is the inverse domain size of the microemulsion structure. The scattering intensity $S(\mathbf{k},t)$ decays exponentially in time t for large t with an algebraic prefactor $t^{-\alpha}$, both in bulk and in film contrast. In the latter case, we find there are several regimes of the wave vector k with different exponents α. [S1063-651X(96)02109-5]

PACS number(s): 61.20.Gy, 64.60.Ht, 82.70.−y

I. INTRODUCTION

Microemulsions in ternary amphiphilic systems have a very intriguing structure on mesoscopic length scales, which gives rise to many interesting properties of these phases [1–3]. It is now well established that for systems containing medium- or long-chain amphiphiles, oil and water channels form two multiply connected networks, which are separated by an amphiphilic monolayer. With decreasing amphiphile chain length, the typical length scale of both the oil and the water domains decreases; simultaneously, the amphiphile concentration within these domains increases. This picture emerges from a series of careful neutron scattering experiments [4–6], together with nuclear magnetic resonance (NMR) self-diffusion measurements [7] and freeze-fracture microscopy [8]. A very similar mesoscopic structure is observed in sponge phases in aqueous amphiphilic solutions, in which an amphiphilic bilayer separates space into two distinct water domains [9,10].

Various theoretical models have been developed during the last few years to understand the properties of microemulsion and sponge phases [2]. Microscopic lattice models and interfacial models have been used, for example, to calculate the scattering intensity in bulk contrast. The calculations show a pronounced peak at nonzero wave vector k, and predict the dependence of the peak position on amphiphile concentration and amphiphile strength [11–13], or on the bending rigidity of an amphiphilic monolayer and the amphiphile concentration [14]. Furthermore, calculations based on Ginzburg-Landau models [15,10,16–18] and on interfacial models [19,20] have shown that the scattering intensity in film contrast shows a characteristic $1/k$ decay for small wave vectors k, followed by a small peak or shoulder at $k \simeq 2q$, where q is the inverse of the typical domain size of the oil or water domains, and finally a $1/k^2$ behavior for $k > 2q$ — in agreement with experimental results [15,21–23].

The complex internal structure of microemulsion and sponge phases should give rise to an interesting dynamical behavior. There have been several studies of the dynamics in these systems, like the calculation of the dynamic scattering intensity in bulk [24,25] and film contrast [26,27], of the viscosity [28] and of the sound attenuation and dispersion [29] — all of which concern dynamical properties of systems in thermal equilibrium —, or the calculation of a sponge-to-lamellar transition in shear flow [30] — a typical nonequilibrium situation.

We want to present in this paper a systematic study of the dynamical behavior of microemulsion and sponge phases in thermal equilibrium. In Sec. II, the time-dependent Ginzburg-Landau model is introduced. In Sec. III, we develop the formalism of the dynamic perturbation theory, and show how the frequency-dependent viscosity $\eta(\omega)$, and the sound velocity $c(\omega)$ and damping $D(\omega)$ can be calculated in this approach. We present the results for the viscoelastic behavior in Sec. IV, and for the sound velocity and damping in Sec. V. In particular, we show that the frequency dependence of these transport coefficients is dominated by a single characteristic frequency ω^*, and discuss the variation of $\eta(\omega)$, $c(\omega)$, $D(\omega)$, and ω^* with the structural parameters — domain size $2\pi/q$ and correlation length ξ — of the static structure of microemulsion and sponge phases. The scattering intensity $S(\mathbf{k},t)$ in bulk and film contrast is calculated in Secs. VI and VII, respectively. In particular, we determine the asymptotic behavior of $S(\mathbf{k},t)$ for short and large times t. The paper closes with a brief summary and discussion in Sec. VIII.

II. GINZBURG-LANDAU MODEL

The basic idea of a description of the dynamics of complex fluids by a Ginzburg-Landau model is to construct differential equations, which determine the temporal evolution of the ''slow'' variables of the system, in particular, all variables which obey a conservation law, while all ''fast'' degrees of freedom are subsumed into a thermal random noise force [31–34]. In the case of fluid ternary amphiphilic mix-

tures, the slow variables are the local concentration difference $\Phi(\mathbf{r},t)$ of oil and water, the local amphiphile concentration $\rho(\mathbf{r},t)$ — or more precisely its deviation from the average amphiphile concentration ρ_s —, the momentum density field $\mathbf{j}(\mathbf{r},t)$, and the pressure field $p(\mathbf{r},t)$. In the case of aqueous amphiphilic solutions, the order parameter $\Phi(\mathbf{r},t)$ is the concentration difference of water on one side (''inside'') and on the other side (''outside'') of the amphiphile bilayer [15]; all other fields have the same meaning as for ternary systems. The dynamics of these fields is governed by the time-dependent Ginzburg-Landau equations [35–37]

$$\frac{\partial\Phi}{\partial t}=-\Gamma_\Phi(i\nabla)^m\frac{\delta\mathcal{F}}{\delta\Phi}+g_0\nabla\left(\Phi\frac{\delta\mathcal{F}}{\delta\mathbf{j}}\right)+\zeta_\Phi, \tag{1}$$

$$\frac{\partial\rho}{\partial t}=\Gamma_\rho\nabla^2\frac{\delta\mathcal{F}}{\delta\rho}+\tau_0\nabla\left(\rho\frac{\delta\mathcal{F}}{\delta\mathbf{j}}\right)+\zeta_\rho, \tag{2}$$

$$\frac{\partial p}{\partial t}=\Gamma_p\nabla^2\frac{\delta\mathcal{F}}{\delta p}+\lambda_0\nabla\frac{\delta\mathcal{F}}{\delta\mathbf{j}}+\zeta_p, \tag{3}$$

$$\frac{\partial\mathbf{j}_T}{\partial t}=\Gamma_T\nabla^2\left(\frac{\delta\mathcal{F}}{\delta\mathbf{j}}\right)_T+g_0\left(\Phi\nabla\frac{\delta\mathcal{F}}{\delta\Phi}\right)_T+\tau_0\left(\rho\nabla\frac{\delta\mathcal{F}}{\delta\rho}\right)_T+\boldsymbol{\zeta}_T, \tag{4}$$

$$\frac{\partial\mathbf{j}_L}{\partial t}=\Gamma_L\nabla^2\left(\frac{\delta\mathcal{F}}{\delta\mathbf{j}}\right)_L+g_0\left(\Phi\nabla\frac{\delta\mathcal{F}}{\delta\Phi}\right)_L+\tau_0\left(\rho\nabla\frac{\delta\mathcal{F}}{\delta\rho}\right)_L+\lambda_0\nabla\frac{\delta\mathcal{F}}{\delta p}+\boldsymbol{\zeta}_L, \tag{5}$$

where the subscripts ''L'' and ''T'' denote the longitudinal and transverse components of a vector field, respectively. The parameter m in Eq. (1) distinguishes the cases of conserved ($m=2$) and nonconserved ($m=0$) order parameter. The thermal random noise forces ζ_Φ, ζ_ρ, ... have a Gaussian probability distribution, with zero average, and the correlations

$$\langle\zeta_\Phi(\mathbf{r},t)\zeta_\Phi(\mathbf{r}',t')\rangle=2\Gamma_\Phi(i\nabla)^m\delta(\mathbf{r}-\mathbf{r}')\delta(t-t'), \tag{6}$$

$$\langle\zeta_\rho(\mathbf{r},t)\zeta_\rho(\mathbf{r}',t')\rangle=-2\Gamma_\rho\nabla^2\delta(\mathbf{r}-\mathbf{r}')\delta(t-t'), \tag{7}$$

$$\langle\zeta_p(\mathbf{r},t)\zeta_p(\mathbf{r}',t')\rangle=-2\Gamma_p\nabla^2\delta(\mathbf{r}-\mathbf{r}')\delta(t-t'), \tag{8}$$

$$\langle\zeta_{T,\alpha}(\mathbf{r},t)\zeta_{T,\beta}(\mathbf{r}',t')\rangle=-2\Gamma_T\nabla^2\delta(\mathbf{r}-\mathbf{r}')\delta(t-t')\delta_{\alpha\beta}, \tag{9}$$

$$\langle\zeta_{L,\alpha}(\mathbf{r},t)\zeta_{L,\beta}(\mathbf{r}',t')\rangle=-2\Gamma_L\nabla^2\delta(\mathbf{r}-\mathbf{r}')\delta(t-t')\delta_{\alpha\beta}. \tag{10}$$

The free-energy functional $\mathcal{F}[\Phi,\rho,p,\mathbf{j}]$, which appears in Eqs. (1)–(5), is given by

$$\mathcal{F}[\Phi,\rho,p,\mathbf{j}]=\mathcal{F}_\Phi[\Phi]+\mathcal{F}_\rho[\rho]+\mathcal{F}_{int}[\Phi,\rho]+\mathcal{F}_{HD}[p,\mathbf{j}]. \tag{11}$$

Here, the first contribution,

$$\mathcal{F}_\Phi=\int d^3r[c(\nabla^2\Phi)^2+g(\Phi)(\nabla\Phi)^2+f(\Phi)], \tag{12}$$

with $c>0$, is the free-energy functional, which has been used extensively for investigations of the static structure and phase behavior of microemulsions [4,38,2]. The functions $f(\Phi)$ and $g(\Phi)$ in Eq. (12) are usually chosen to have the form

$$g(\Phi)=b_0+b_2\Phi^2, \tag{13}$$

$$f(\Phi)=r_2\Phi^2+r_4\Phi^4+r_6\Phi^6, \tag{14}$$

with $b_2\geqslant 0$, $r_2>0$ and $r_6\geqslant 0$. The important features of these functions are that $f(\Phi)$ has three minima, which correspond to the three homogeneous phases oil-rich, water-rich, and microemulsion, and that $g(0)<0$, so that the scattering intensity of the microemulsion (with $\langle\Phi\rangle=0$) in bulk contrast has a pronounced peak at wave vector $k>0$. The latter property can be seen from an explicit calculation of the scattering intensity $\chi_0(k)$ in the Ornstein-Zernike approximation, which yields [4,38]

$$\chi_0(k)=\frac{1}{2}[ck^4+b_0k^2+r_2]^{-1}. \tag{15}$$

The Fourier transform of Eq. (15) is the real-space correlation function [4]

$$G(r)\sim\frac{1}{r}e^{-r/\xi}\sin(qr) \tag{16}$$

with

$$\xi^{-2}=(r_2/4c)^{1/2}+(b_0/4c),\quad q^2=(r_2/4c)^{1/2}-(b_0/4c). \tag{17}$$

The oscillatory exponential decay of $G(r)$ demonstrates that the structure of a microemulsion is characterized by *two* independent length scales, the correlation length ξ and the inverse average domain size q. The dimensionless product $q\xi$ is a convenient measure of the structure of a microemulsion. Weakly structured microemulsions with $0<q\xi<1$ have an oscillatory correlation function, but no peak in the scattering intensity at nonzero wave vector k. The peak in $\chi_0(k)$ for $k>0$ appears at $q\xi=1$, and becomes more pronounced with increasing $q\xi$.

Since we are mainly interested in the properties of the microemulsion or sponge phase, and not in their coexistence with other phases, we choose for f and g the simple form

$$g(\Phi)=b_0,\quad f(\Phi)=r_2\Phi^2, \tag{18}$$

i.e., we ignore higher-than-quadratic terms in the free-energy functional (12).

Although the local amphiphile concentration does not appear in the model (12), the *average* amphiphile concentration

ρ_s enters as a parameter; the value of b_0, for example, decreases with increasing ρ_s. The model (12), with only a single order parameter field Φ, already describes many properties of microemulsions, such as their wetting behavior at the oil-water interface [38–42]. However, in some cases it is necessary or convenient to take into account the local amphiphile concentration explicitly. In this case, the free-energy functional has two additional contributions,

$$\mathcal{F}_\rho = \int d^3r[\,\gamma(\nabla^2\rho)^2+\beta(\nabla\rho)^2+\alpha\rho^2], \tag{19}$$

with $\gamma>0$, $\beta>0$ and $\alpha>0$, and [10,16]

$$\mathcal{F}_{int} = \int d^3r[\,\beta_1\rho\Phi^2+\beta_2(\nabla^2\rho)\Phi^2+\beta_3\rho\Phi(\nabla^2\Phi)]. \tag{20}$$

The coupling terms in Eq. (20) between the two order parameters include only the lowest powers of ρ and Φ which are allowed by symmetry arguments in a balanced microemulsion, and at most two spatial derivatives of the fields. This model for Φ and ρ has been used to calculate the scattering intensity in film contrast [15,16], and first showed all the essential characteristics of this intensity described in the introduction. Finally, the ''hydrodynamic'' part of the free-energy functional (11) takes the form [43]

$$\mathcal{F}_{HD} = \int d^3r\left[\frac{1}{2}p^2+\frac{1}{2}\mathbf{j}^2\right]. \tag{21}$$

We now return to the form of the time-dependent Ginzburg-Landau equations (1)–(5) to comment on the physical interpretation of the various terms. The first term on the right-hand side (rhs) of Eq. (4) together with the left-hand side (lhs) is the transverse component of the linearized Navier-Stokes equation; similarly, the first and fourth terms on the rhs of Eq. (5) together with the lhs can be identified with its longitudinal component. The first term on the rhs of Eq. (1) with $m=2$ describes the diffusion of the order parameter Φ in microemulsions, or in sponge phases with an impenetrable bilayer, since in both cases the order parameter is conserved. The order parameter is *not* conserved, on the other hand, in sponge phases in which water can leak through the amphiphilic bilayer; in this case $m=0$. The second terms on the rhs of Eqs. (1) and (2) describe the change of concentrations due to fluid flow; thus, these terms can be understood as a continuity equation. The second and third terms on the rhs of Eqs. (4) and (5) represent structural forces, which are necessary to fulfill detailed balance [44,45]. Finally, Eq. (3) for the pressure field corresponds to the continuity equation for the total mass density.

Note that the *fluctuation-dissipation theorem* [46,47] requires that the coefficients in the noise correlations (6)–(10) are identical with the *dissipative* or *irreversible* coupling constants Γ_Φ, Γ_ρ, Γ_T, and Γ_L. Detailed balance also requires that the *reversible* coupling constants — g_0, λ_0, and τ_0 — of ''corresponding'' terms, like the $\nabla\delta\mathcal{F}/\delta\mathbf{j}$ contribution in Eq. (3) for p, and the $\nabla\delta\mathcal{F}/\delta p$ contribution in Eq. (5) for $\mathbf{j}_L$, are the same.

Finally, we want to mention that time-dependent Ginzburg-Landau equations have been studied intensively in the context of dynamic critical phenomena [48,35]. Two limiting cases of Eqs. (1)–(5) have been investigated in particular: model H [49,35], which is given by Eqs. (1) and (4) — with $\tau_0=0$ —, and model C [50,35], which is defined by Eqs. (1) and (2) — with $g_0=\tau_0=0$. The free-energy functionals $\mathcal{F}$ for critical phenomena and for ternary amphiphilic systems are quite different, however, so that the same equations of motion will give rise to a markedly different dynamical behavior.

III. DYNAMIC PERTURBATION THEORY

The fundamental quantities of interest, which characterize the dynamical behavior of the system in thermal equilibrium, are the correlation functions

$$C_{ij}(\mathbf{r}-\mathbf{r}',t-t') = \langle\Psi_i(\mathbf{r},t)\Psi_j(\mathbf{r}',t')\rangle, \tag{22}$$

where $\Psi_i\in\{\Phi,\rho,p,\mathbf{j}_T,\mathbf{j}_L\}$, and the response functions $R_{ij}(\mathbf{r}-\mathbf{r}',t-t')$, which describe the response of the system at time t to a (small) external perturbation at time t'. In order to calculate these quantities, it turns out to be very convenient to introduce ''response fields'' $\tilde{\Psi}_i(\mathbf{r},t)$ [51,52,34]. One of the advantages of these additional fields is that the response functions can now be calculated on the same level as the correlation functions by an equilibrium average,

$$R_{ij}(\mathbf{r}-\mathbf{r}',t-t') = \langle\Psi_i(\mathbf{r},t)\tilde{\Psi}_j(\mathbf{r}',t')\rangle \propto \theta(t-t'). \tag{23}$$

Both correlation and response functions can be obtained from the generating functional

$$\begin{aligned} Z[l_\Phi,\tilde{l}_\Phi,l_\rho,\tilde{l}_\rho,l_p,\tilde{l}_p,\mathbf{l}_{\mathbf{j}_T},\tilde{\mathbf{l}}_{\mathbf{j}_T},\mathbf{l}_{\mathbf{j}_L},\tilde{\mathbf{l}}_{\mathbf{j}_L}] = \int\mathcal{D}\Phi\int\mathcal{D}(i\tilde{\Phi})\int\mathcal{D}\rho\int\mathcal{D}(i\tilde{\rho})\int\mathcal{D}p\int\mathcal{D}(i\tilde{p})\int\mathcal{D}\mathbf{j}_T\int\mathcal{D}(i\tilde{\mathbf{j}}_T)\int\mathcal{D}\mathbf{j}_L\int\mathcal{D}(i\tilde{\mathbf{j}}_L) \\ \times\exp\Big\{\mathcal{A}[\Phi,\tilde{\Phi},\rho,\tilde{\rho},p,\tilde{p},\mathbf{j}_T,\tilde{\mathbf{j}}_T,\mathbf{j}_L,\tilde{\mathbf{j}}_L]+\int dt\int d^3r[\,l_\Phi\Phi+\tilde{l}_\Phi\tilde{\Phi}+l_\rho\rho+\tilde{l}_\rho\tilde{\rho}+l_p p+\tilde{l}_p\tilde{p} \\ +\mathbf{l}_{\mathbf{j}_T}\mathbf{j}_T+\tilde{\mathbf{l}}_{\mathbf{j}_T}\tilde{\mathbf{j}}_T+\mathbf{l}_{\mathbf{j}_L}\mathbf{j}_L+\tilde{\mathbf{l}}_{\mathbf{j}_L}\tilde{\mathbf{j}}_L]\Big\} \end{aligned} \tag{24}$$

with the ''action''

$$\mathcal{A}=\int dt\int d^3r\Bigg\{-\widetilde{\Phi}\Gamma_\Phi(i\nabla)^m\widetilde{\Phi}+\widetilde{\rho}\Gamma_\rho\nabla^2\widetilde{\rho}+\widetilde{p}\Gamma_p\nabla^2\widetilde{p}+\widetilde{\mathbf{j}}_T\Gamma_T\nabla^2\widetilde{\mathbf{j}}_T+\widetilde{\mathbf{j}}_L\Gamma_L\nabla^2\widetilde{\mathbf{j}}_L+\widetilde{\Phi}\left[\frac{\partial\Phi}{\partial t}+\Gamma_\Phi(i\nabla)^m\frac{\delta\mathcal{F}}{\delta\Phi}-g_0\nabla(\Phi\mathbf{j})\right]$$
$$+\widetilde{\rho}\left[\frac{\partial\rho}{\partial t}-\Gamma_\rho\nabla^2\frac{\delta\mathcal{F}}{\delta\rho}-\tau_0\nabla(\rho\mathbf{j})\right]+\widetilde{p}\left[\frac{\partial p}{\partial t}-\Gamma_p\nabla^2p-\lambda_0\nabla\mathbf{j}_L\right]+\widetilde{\mathbf{j}}_T\left[\frac{\partial\mathbf{j}_T}{\partial t}-\Gamma_T\nabla^2\mathbf{j}_T-g_0\left(\Phi\nabla\frac{\delta\mathcal{F}}{\delta\Phi}\right)_T-\tau_0\left(\rho\nabla\frac{\delta\mathcal{F}}{\delta\rho}\right)_T\right]$$
$$+\widetilde{\mathbf{j}}_L\left[\frac{\partial\mathbf{j}_L}{\partial t}-\Gamma_L\nabla^2\mathbf{j}_L-\lambda_0\nabla p-g_0\left(\Phi\nabla\frac{\delta\mathcal{F}}{\delta\Phi}\right)_L-\tau_0\left(\rho\nabla\frac{\delta\mathcal{F}}{\delta\rho}\right)_L\right]\Bigg\}, \tag{25}$$

where

$$\frac{\delta\mathcal{F}}{\delta\Phi}=2(c\nabla^4-b_0\nabla^2+r_2)\Phi+2\beta_1\rho\Phi+2\beta_2(\nabla^2\rho)\Phi+\beta_3[\rho\nabla^2\Phi+\nabla^2(\rho\Phi)] \tag{26}$$

and

$$\frac{\delta\mathcal{F}}{\delta\rho}=2(\gamma\nabla^4-\beta\nabla^2+\alpha)\rho+\beta_1\Phi^2+\beta_2\nabla^2\Phi^2+\beta_3\Phi\nabla^2\Phi. \tag{27}$$

The generating functional (24) defines an analog of the partition function of equilibrium statistical mechanics. This form of the time-dependent Ginzburg-Landau equations has the advantage that all the tools of field-theoretic perturbation theory, as developed for static Ginzburg-Landau models, can be employed.

The perturbation theory is set up by first neglecting all terms of higher-than-quadratic order in the action. In this case, the Gaussian action $\mathcal{A}_0$ takes in Fourier space the form

$$\mathcal{A}_0=\int\frac{d\omega}{2\pi}\int\frac{d^3k}{(2\pi)^3}A_0(\mathbf{k},\omega), \tag{28}$$

with

$$A_0(\mathbf{k},\omega)=\frac{1}{2}\mathbf{\Psi}^T(\mathbf{k},\omega)[G^{(0)}]^{-1}\mathbf{\Psi}(-\mathbf{k},-\omega), \tag{29}$$

where the vector $\mathbf{\Psi}$ of the dynamic fields is defined by

$$\mathbf{\Psi}^T\equiv(\widetilde{\Phi},\Phi,\widetilde{\rho},\rho,\widetilde{\mathbf{j}}_T,\mathbf{j}_T,\widetilde{\mathbf{j}}_L,\widetilde{p},\mathbf{j}_L,p) \tag{30}$$

(the superscript ''T'' denotes the transposition of a vector). The 10×10 matrix $[G^{(0)}]^{-1}$ is composed of three 2×2 blocks and one 4×4 block along the diagonal,

$$[G^{(0)}]^{-1}=\begin{pmatrix}[G^{(0)}]^{-1}\{\widetilde{\Phi},\Phi\} & 0 & 0 & 0\\ 0 & [G^{(0)}]^{-1}\{\widetilde{\rho},\rho\} & 0 & 0\\ 0 & 0 & [G^{(0)}]^{-1}\{\widetilde{\mathbf{j}}_T,\mathbf{j}_T\} & 0\\ 0 & 0 & 0 & [G^{(0)}]^{-1}\{\widetilde{\mathbf{j}}_L,\widetilde{p},\mathbf{j}_L,p\}\end{pmatrix}. \tag{31}$$

The block matrices are easily obtained from Eq. (25), and are given by

$$[G^{(0)}]^{-1}\{\widetilde{\Phi},\Phi\}=\begin{pmatrix}-2\Gamma_\Phi k^m & i\omega+\Gamma_\Phi k^m\chi_0^{-1}(k)\\ -i\omega+\Gamma_\Phi k^m\chi_0^{-1}(k) & 0\end{pmatrix}, \tag{32}$$

where $\chi_0(k)$ is the static scattering intensity in bulk contrast, see Eq. (15),

$$[G^{(0)}]^{-1}\{\widetilde{\rho},\rho\}=\begin{pmatrix}-2\Gamma_\rho k^2 & i\omega+\Gamma_\rho k^2\chi_\rho^{-1}(k)\\ -i\omega+\Gamma_\rho k^2\chi_\rho^{-1}(k) & 0\end{pmatrix}, \tag{33}$$

where

$$\chi_\rho(k)=[2(\gamma k^4+\beta k^2+\alpha)]^{-1} \tag{34}$$

is the static scattering intensity of the amphiphile in the Ornstein-Zernike approximation,

$$[G^{(0)}]^{-1}\{\tilde{\mathbf{j}}_T,\mathbf{j}_T\}=\begin{pmatrix} -2\Gamma_T k^2 & i\omega+\Gamma_T k^2 \\ -i\omega+\Gamma_T k^2 & 0 \end{pmatrix}, \tag{35}$$

and

$$[G^{(0)}]^{-1}\{\tilde{\mathbf{j}}_L,\tilde{p},\mathbf{j}_L,p\}=\begin{pmatrix} -2\Gamma_L k^2 & 0 & i\omega+\Gamma_L k^2 & i\lambda_0\mathbf{k} \\ 0 & -2\Gamma_p k^2 & i\lambda_0\mathbf{k} & i\omega+\Gamma_p k^2 \\ -i\omega+\Gamma_L k^2 & -i\lambda_0\mathbf{k} & 0 & 0 \\ -i\lambda_0\mathbf{k} & -i\omega+\Gamma_p k^2 & 0 & 0 \end{pmatrix}. \tag{36}$$

The inversion of the matrix $[G^{(0)}]^{-1}$ gives all correlation and response functions in the Gaussian (or van-Hove) approximation. Due to the block structure, the inversion is straightforward; a complete list of the results can be found in Appendix A.

The next step is to take into account the nonlinear terms in the time-dependent Ginzburg-Landau equations, which are equivalent to higher-than-quadratic terms in the dynamic action (25). These terms lead to a coupling of the independent modes of the Gaussian approximation. Note that this coupling is essential for the investigation of the dynamics of microemulsions and sponge phases, since only due to the nonlinear terms can the hydrodynamic modes be affected by the structure.

The matrix G of the full correlation and response functions can be written as an infinite series of Feynman diagrams. A partial summation of this series is possible by the Dyson equation,

$$G^{-1}(\mathbf{k},\omega)=[G^{(0)}]^{-1}(\mathbf{k},\omega)-\Sigma(\mathbf{k},\omega). \tag{37}$$

The advantage of this (exact) relation is that only *one-particle-irreducible* Feynman diagrams, i.e., diagrams which do not separate into two disconnected pieces by cutting a line, contribute to the self-energy matrix $\Sigma(\mathbf{k},\omega)$. It can now be shown that — due to the structure of the Langevin equations (1)–(5) — the self-energy matrix has the same block structure as the Gaussian correlation and response matrix $[G^{(0)}]^{-1}$. Furthermore, the lower right corner of these block matrices vanishes identically due to causality, just as in the Gaussian matrices (32)–(36). Thus the inversion of G^{-1} is just as simple as the inversion of $[G^{(0)}]^{-1}$.

The quantities we are mainly interested in are the scattering intensities, the viscosity, and the sound attenuation and dispersion of a microemulsion or sponge phase. The scattering intensity in bulk contrast is obtained from the Dyson equation to be

$$G_{\Phi\Phi}(\mathbf{k},\omega)=\frac{2\Gamma_\Phi k^m+\Sigma_{\tilde{\Phi}\tilde{\Phi}}(\mathbf{k},\omega)}{|-i\omega+\Gamma_\Phi k^m\chi_0^{-1}(k)-\Sigma_{\Phi\tilde{\Phi}}(\mathbf{k},\omega)|^2}; \tag{38}$$

similarly, the amphiphile scattering intensity is found to be

$$G_{\rho\rho}(\mathbf{k},\omega)=\frac{2\Gamma_\rho k^2+\Sigma_{\tilde{\rho}\tilde{\rho}}(\mathbf{k},\omega)}{|-i\omega+\Gamma_\rho k^2\chi_\rho^{-1}(k)-\Sigma_{\rho\tilde{\rho}}(\mathbf{k},\omega)|^2}. \tag{39}$$

It is important to note at this point that the fluctuation-dissipation theorem (FDT) poses strong constraints on the form of the self-energy matrix. As explained in Appendix B, the FDT implies

$$\Sigma_{\tilde{\Phi}\tilde{\Phi}}(\mathbf{k},\omega)=-2\chi_0(k)\mathrm{Re}\{\Sigma_{\Phi\tilde{\Phi}}(\mathbf{k},\omega)\} \tag{40}$$

and similarly for $\Sigma_{\tilde{\rho}\tilde{\rho}}(\mathbf{k},\omega)$. Thus, in order to calculate the scattering intensities (38) and (39), only the self-energies $\Sigma_{\Phi\tilde{\Phi}}(\mathbf{k},\omega)$ and $\Sigma_{\rho\tilde{\rho}}(\mathbf{k},\omega)$ have to be evaluated, respectively.

The viscosity $\eta(\omega)$ follows from the pole structure of the correlation and response functions of the transverse momentum density in the *hydrodynamic limit* $k\to 0$. For the response function, Eq. (35) together with the self-energy contributions implies

$$G_{\tilde{\mathbf{j}}_T\mathbf{j}_T}(\mathbf{k},\omega)=\frac{1}{-i\omega+\Gamma_T k^2-\Sigma_{\tilde{\mathbf{j}}_T\tilde{\mathbf{j}}_T}(\mathbf{k},\omega)}. \tag{41}$$

This result can now be compared with the dispersion relation

$$-i\omega+\frac{\eta}{\rho_m}k^2=0, \tag{42}$$

where ρ_m is the mass density, which follows from the analysis of the Navier-Stokes equation. In order to simplify the notation, we absorb the mass density into η, so that from now on η is the kinematic viscosity. This yields

$$\eta(\omega)=\Gamma_T-\frac{\partial}{\partial k^2}\Sigma_{\tilde{\mathbf{j}}_T\tilde{\mathbf{j}}_T}(\mathbf{k},\omega)\bigg|_{k=0}. \tag{43}$$

Note that when the nonlinear terms in Eqs. (1)–(5) are neglected, the viscosity is frequency independent; furthermore, η has no imaginary part in this case, i.e., there is no elastic response to an external oscillatory shear force.

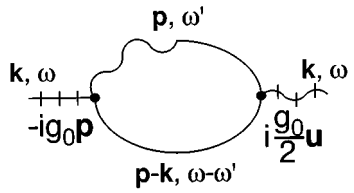

FIG. 1. Feynman diagram for the self-energy $\Sigma_{\mathbf{j}_T\tilde{\mathbf{j}}_T}(\mathbf{k},\omega)$ in a one-loop approximation. The notation for the various propagators and vertices is explained in Appendix A. The contribution of the right vertex contains the vector $\mathbf{u}=(\mathbf{p}-\mathbf{k})\chi_0^{-1}(\mathbf{p}-\mathbf{k})-\mathbf{p}\chi_0^{-1}(p)$.

Sound waves determine the pole structure of the correlation and response functions of the pressure and of the longitudinal momentum density in the hydrodynamic limit. Thus the dispersion relation of a sound wave is given by the zeros of the denominator of these correlation and response functions,

$$\det([G^{(0)}]^{-1}\{\tilde{\mathbf{j}}_L,\tilde{p},\mathbf{j}_L,p\}-\Sigma\{\tilde{\mathbf{j}}_L,\tilde{p},\mathbf{j}_L,p\})=0. \quad (44)$$

Due to the special structure of the matrix (36) — and of the corresponding part of the Σ matrix —, this equation reduces to

$$\det\begin{pmatrix} -i\omega+\Gamma_L k^2-\Sigma_{\mathbf{j}_L\tilde{\mathbf{j}}_L}(\mathbf{k},\omega) & -i\lambda_0\mathbf{k}-\Sigma_{\mathbf{j}_L\tilde{p}}(\mathbf{k},\omega) \\ -i\lambda_0\mathbf{k}-\Sigma_{p\tilde{\mathbf{j}}_L}(\mathbf{k},\omega) & -i\omega+\Gamma_p k^2-\Sigma_{p\tilde{p}}(\mathbf{k},\omega)\end{pmatrix} =0. \quad (45)$$

To proceed, we have to determine the leading powers of all self-energies appearing in Eq. (45) in the hydrodynamic limit $k\to 0$. This can only be done by considering explicitly the Feynman diagrams for these self-energies. In the one-loop approximation, we find

$$\Sigma_{\mathbf{j}_L\tilde{\mathbf{j}}_L}\sim\mathcal{O}(k^2),\quad \Sigma_{p\tilde{\mathbf{j}}_L}\sim\mathcal{O}(k^3),\quad \Sigma_{\mathbf{j}_L\tilde{p}}\sim\mathcal{O}(k^3),\quad \Sigma_{p\tilde{p}}\sim\mathcal{O}(k^4). \quad (46)$$

Thus, only $\Sigma_{\mathbf{j}_L\tilde{\mathbf{j}}_L}$ contributes to order k^2, so that

$$-\omega^2+\lambda_0^2k^2-i\omega k^2\left[\Gamma_L+\Gamma_p-\frac{\partial}{\partial k^2}\Sigma_{\mathbf{j}_L\tilde{\mathbf{j}}_L}(\mathbf{k},\omega)\bigg|_{k=0}\right]+\mathcal{O}(k^4)=0. \quad (47)$$

On the other hand, a sound wave with wave vector k, velocity $c(\omega)$, and damping constant $D(\omega)$ obeys the dispersion relation [47]

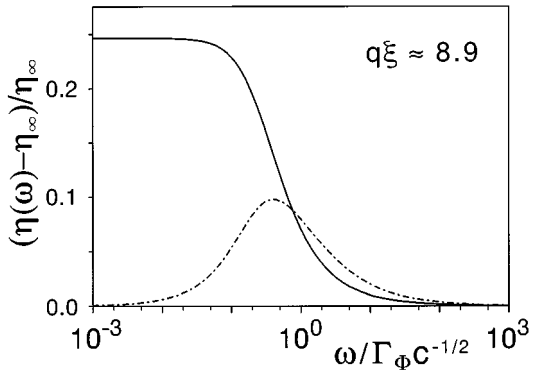

FIG. 2. Real and imaginary part of the complex viscosity η as a function of the scaled frequency $\omega/(\Gamma_\Phi c^{-1/2})$, for a system with conserved order parameter Φ. The parameters are $g_0=1$, $\Gamma_\Phi=1$, $c=1$, $b_0=-1.95$, and $r_2=1$ (so that $q\xi\simeq 8.9$).

$$\omega^2-c(\omega)^2k^2+i\omega D(\omega)k^2=0. \quad (48)$$

The comparison of Eqs. (47) and (48) finally gives [53]

$$c^2(\omega)=\lambda_0^2-\omega\,\mathrm{Im}\left(\frac{\partial}{\partial k^2}\Sigma_{\mathbf{j}_L\tilde{\mathbf{j}}_L}(\mathbf{k},\omega)\bigg|_{k=0}\right), \quad (49)$$

$$D(\omega)=\Gamma_p+\Gamma_L-\mathrm{Re}\left(\frac{\partial}{\partial k^2}\Sigma_{\mathbf{j}_L\tilde{\mathbf{j}}_L}(\mathbf{k},\omega)\bigg|_{k=0}\right). \quad (50)$$

Note that, as in the case of the viscosity, when the nonlinear terms in the Langevin equations are neglected, both the sound velocity and the damping are frequency independent. Since the derivative of the self-energy with respect to k^2 will appear frequently in the following sections, we introduce the notation

$$\gamma_{\mathbf{j}_T\tilde{\mathbf{j}}_T}(\omega)\equiv\frac{\partial}{\partial k^2}\Sigma_{\mathbf{j}_T\tilde{\mathbf{j}}_T}(\mathbf{k},\omega)\bigg|_{k=0} \quad (51)$$

and similarly $\gamma_{\mathbf{j}_L\tilde{\mathbf{j}}_L}(\omega)$.

IV. VISCOELASTICITY

It has been shown in Sec. III that the viscosity is related to the self-energy $\Sigma_{\mathbf{j}_T\tilde{\mathbf{j}}_T}(\mathbf{k},\omega)$ in the limit $k\to 0$. The leading contribution to this self-energy term is the one-loop diagram shown in Fig. 1. Inserting the expressions for the propagators and vertices given in Appendix A, we obtain the explicit result

$$\Sigma_{\mathbf{j}_T\tilde{\mathbf{j}}_T}(\mathbf{k},\omega)=g_0^2\int\frac{d^3p}{(2\pi)^3}\,\frac{\chi_0^{-1}(\mathbf{p}-\mathbf{k})-\chi_0^{-1}(p)}{\chi_0^{-1}(\mathbf{p}-\mathbf{k})}\,\frac{\mathbf{p}\cdot\mathcal{T}_k\cdot\mathbf{p}}{-i\omega+\Gamma_\Phi p^2\chi_0^{-1}(p)+\Gamma_\Phi(\mathbf{p}-\mathbf{k})^2\chi_0^{-1}(\mathbf{p}-\mathbf{k})}, \quad (52)$$

where $[\mathcal{T}_k]_{\alpha\beta} \equiv \delta_{\alpha\beta} - k_\alpha k_\beta / k^2$ is the transverse projector (so that $\mathcal{T}_k \cdot \mathbf{k} = 0$). Here, the integral over the internal frequency ω' (compare Fig. 1) has already been carried out. An expansion of Eq. (52) in powers of $\mathbf{k}$, and a subsequent integration over the angular components yields

$$\gamma_{\tilde{\mathbf{j}}_T \tilde{\mathbf{j}}_T}(\omega) = \frac{2g_0^2}{15\pi^2} \int_0^\infty dp \frac{p^4}{\chi_0^{-1}(p)[-i\omega + 2\Gamma_\Phi p^2 \chi_0^{-1}(p)]} \times \Bigg\{ (5b_0 + 14cp^2) + \frac{4h(p)p^2}{\chi_0^{-1}(p)[-i\omega + 2\Gamma_\Phi p^2 \chi_0^{-1}(p)]} \times \{ i2h(p)\omega - \Gamma_\Phi \chi_0^{-1}(p)[6h(p)p^2 + \chi_0^{-1}(p)] \} \Bigg\}, \tag{53}$$

where

$$h(p) \equiv b_0 + 2cp^2. \tag{54}$$

Except for the case $\omega = 0$, the integration over the internal wave vector p has to be done numerically. A typical result for the viscosity $\eta(\omega)$ of a strongly structured microemulsion, with $q\xi \simeq 8.9$, is shown in Fig. 2. Here, the viscosity in the high frequency limit, $\eta_\infty = \lim_{\omega \to \infty} \eta(\omega) = \Gamma_T$, has been subtracted. The curves show the typical behavior of complex fluids. The real part of η is approximately frequency independent for small ω, i.e., the fluid behaves Newtonian. At a characteristic frequency ω^*, the real part of η drops sharply; the imaginary part shows a peak in the same frequency range. A very similar behavior has been found, for example, in dense colloidal suspensions [54,55].

This behavior of $\eta(\omega)$ can be understood as follows. For very small frequencies, the system has enough time to relax the stress which builds up due to the external shearing force by rebuilding its internal structure such as to stay as close to its equilibrium state as possible. This process is accompanied by a lot of energy dissipation, but allows little elastic response. At higher frequencies, near the characteristic frequency ω^*, the structural relaxation is no longer fast enough to follow the external shear stress, so that energy can now be stored elastically. Finally, for very high frequencies, the viscosity of the fluid is dominated by the viscosity of the solvent.

The analysis of Eq. (53) shows that the viscosity can be written in the scaling form

$$\frac{\eta(\omega) - \eta_\infty}{\eta_\infty} = \frac{g_0^2}{\Gamma_\Phi \Gamma_T c^{1/4}} \overline{\xi}^3 V\left(q\xi, \frac{\omega}{\omega_v^*} \right), \tag{55}$$

where

$$\overline{\xi} = c^{-1/4} \xi \tag{56}$$

is the correlation length measured in units of the ''amphiphile length'' $c^{1/4}$. The characteristic frequency ω_v^* in Eq. (55), which is defined by the location of the maximum of $\mathrm{Im}(\eta)$, also shows scaling behavior,

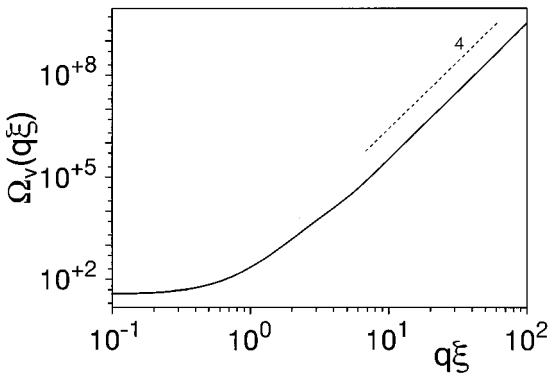

FIG. 3. Scaling function $\Omega_v(q\xi)$ of the characteristic frequency ω_v^* for conserved order parameter Φ.

$$\omega_v^* = (\Gamma_\Phi c^{-1/2}) \overline{\xi}^{-6} \Omega_v(q\xi). \tag{57}$$

These scaling forms indicate the most interesting aspect of the viscosity of microemulsions and sponge phases, which is its dependence on the structural parameters q and ξ.

In the case $\omega = 0$, the scaling function V of Eq. (55) can be calculated analytically,

$$V(y, \omega = 0) = \frac{1}{240\pi} \frac{1 + \frac{1}{4}y^2}{1 + y^2}. \tag{58}$$

This result for the *zero-shear viscosity* agrees with the result of Mundy, Levin, and Dawson [28,56], which has been obtained from the somewhat different approach of Fredrickson and Larson [57], who studied the linear response of the system to an external shear stress. Since the dependence of $V(q\xi, \omega = 0)$ on the dimensionless parameter $q\xi$ is rather weak, the behavior of the zero-shear viscosity is dominated by the $\overline{\xi}^3$ prefactor in Eq. (55). Thus the zero-shear viscosity should increase rapidly as the transition to a spatially ordered phase — such as a lamellar or a cubic bicontinuous phase — is approached. The origin of this increase can be understood intuitively: with increasing ξ, the size of coherent, well-ordered regions in the microemulsion becomes larger and larger; therefore, more and more energy is dissipated when the structure within these regions is rearranged.

The scaling function $\Omega_v(q\xi)$ of the characteristic frequency is shown in Fig. 3. The expression

$$\Omega_v(q\xi) = 32.5[1 + 4.5(q\xi)^2 + (q\xi)^4] \tag{59}$$

contains the leading power-law behaviors for both small and large values of $q\xi$, and fits the curve shown in Fig. 3 over the whole range of the argument quite well. Thus the structural relaxation time $1/\omega_v^*$ increases with increasing correlation length *and* with increasing domain size $2\pi/q$. The origin of this behavior can again be understood intuitively: the larger the size of an ordered region, the longer it takes to rearrange its structure.

The full scaling function $V(q\xi, \omega/\omega_v^*)$ has to be calculated numerically; its real and imaginary parts are shown in Fig. 4. The strongest frequency dependence of both the real and the imaginary part of V occurs at the disorder line

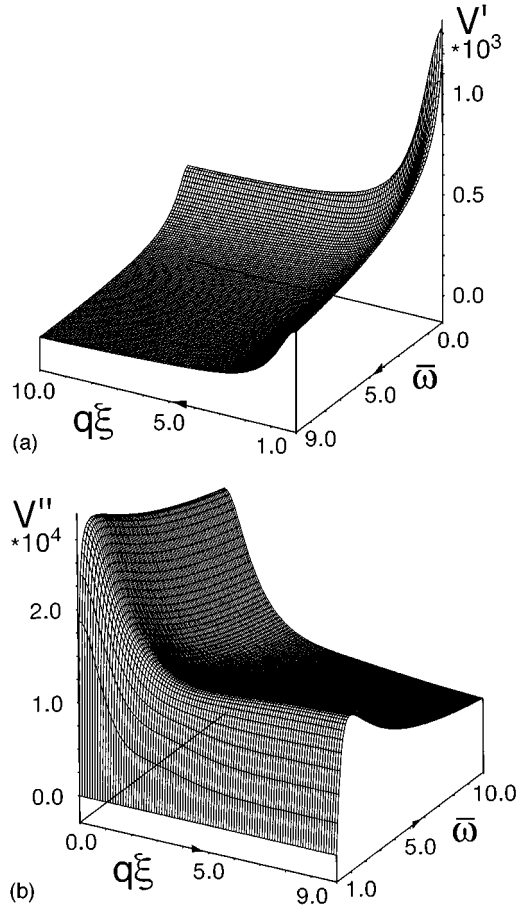

FIG. 4. (a) Real and (b) imaginary part of the scaling function $V(q\xi,\overline{\omega})$ of the complex viscosity, with $\overline{\omega}=\omega/\omega_v^*$

$(q\xi=0)$. This does not indicate, however, that the viscoelasticity of an unstructured fluid varies strongly as a function of ω; the prefactor $\overline{\xi^3}$ in Eq. (55) rather leads to a decreasing frequency dependence with decreasing structure. This is again in qualitative agreement with colloidal suspensions [58].

The behavior of $V(q\xi,\omega/\omega_v^*)$ for $\omega\ll\omega_v^*$ can be studied analytically. In this limit, one finds the power laws

$$\left.\begin{aligned}\mathrm{Re}[V(\cdot,0)-V(\cdot,\overline{\omega})]&\sim\overline{\omega^2}\\ \mathrm{Im}[V(\cdot,\overline{\omega})]&\sim\overline{\omega}\end{aligned}\right\}\ \overline{\omega}\to 0. \tag{60}$$

This result can be used to obtain the *storage and loss moduli* $G'(\omega)=\omega\mathrm{Im}[\eta(\omega)]$ and $G''(\omega)=\omega\mathrm{Re}[\eta(\omega)-\eta_\infty]$ in the low-frequency limit,

$$G'(\omega)=\frac{g_0^2\xi^9}{30720\pi\Gamma_\Phi^2c^2}\,\frac{14+(q\xi)^2+4(q\xi)^4+(q\xi)^6}{[1+(q\xi)^2]^5}\,\omega^2 \tag{61}$$

and

$$G''(\omega)=\frac{g_0^2\xi^3}{960\pi\Gamma_\Phi c}\,\frac{4+(q\xi)^2}{1+(q\xi)^2}\,\omega. \tag{62}$$

The same ω-power laws and the same divergence of the prefactors in the limit $\xi\to\infty$ (with q fixed) have been obtained for diblock copolymer melts by Fredrickson and Larson [57,59] with a different formalism. Since in both theories the behavior of the viscosity is determined by the *static* structure factor, which has a very similar form for microemulsions and diblock copolymers (in the weak-segregation regime) [60,61], we believe that our other results for the viscosity, like the scaling behavior of the characteristic frequency Eq. (57) and for the sound attenuation and dispersion curves to be discussed in the next section, should also apply to disordered diblock copolymers.

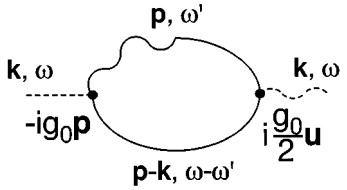

FIG. 5. Feynman diagram for the self-energy $\Sigma_{\mathbf{j}_L\tilde{\mathbf{j}}_L}(\mathbf{k},\omega)$ in a one-loop approximation. The notation for the various propagators and vertices is explained in Appendix A. The contribution of the right vertex contains the vector $\mathbf{u}=(\mathbf{p}-\mathbf{k})\chi_0^{-1}(\mathbf{p}-\mathbf{k})-\mathbf{p}\chi_0^{-1}(p)$.

The results (62) and (61) for the frequency dependence of the storage and loss moduli can be used to define another characteristic frequency,

$$\omega_G^*\equiv\lim_{\omega\to 0}\frac{\omega G''(\omega)}{G'(\omega)}=(\Gamma_\Phi c^{-1/2})\overline{\xi^{-6}}\Omega_G(q\xi), \tag{63}$$

where the scaling function Ω_G is given by

$$\Omega_G(y)=32\frac{(4+y^2)(1+y^2)^4}{14+y^2+4y^4+y^6}. \tag{64}$$

This result can now be compared with the characteristic frequency ω_v^* Eqs. (57) and (59). The two functions have a different form for small $q\xi$, but agree very well for $q\xi\geqslant 2$, i.e., for sufficiently well structured microemulsions. We conclude that in strongly structured microemulsions, the small-ω behavior of the viscosity is dominated by a *single* structural relaxation time.

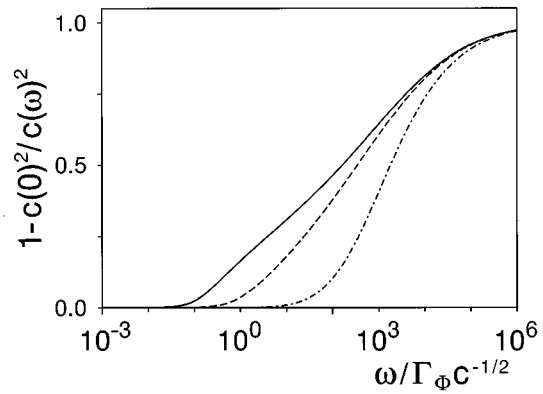

FIG. 6. Sound dispersion $\Delta(\omega)$ for $q=0.95$ and $\xi=1.0$ (dashed-dotted line), $\xi=5.0$ (dashed line), $\xi=11.0$ (full line). The parameters are $c=1$, $g_0=1$, and $\lambda_0=1$.

Expression (52) for the self-energy shows that the characteristic frequency ω^* is determined by the relaxation times of the order parameter fluctuations. For strongly structured microemulsions, their dynamics is dominated by the modes with wave vectors in the vicinity of the inverse domain size, q, which have the longest relaxation times.

Finally, the behavior of V for large frequencies is found numerically to be

$$V(;\overline{\omega}) \sim \overline{\omega}^{-1/2}, \quad \overline{\omega} \to \infty. \tag{65}$$

The same frequency dependence has been observed in other strongly structured complex fluids, such as in hard-sphere colloidal suspensions (both theoretically [54] and experimentally [55]), and in polymer solutions in the Rouse regime [62].

So far, we have completely neglected the contribution of the fluctuations of the amphiphile concentration ρ to the viscosity. In fact, in addition to the diagram shown in Fig. 1, there is a second, analogous diagram, in which the internal lines are replaced by ρ correlation and response propagators. The structure of this contribution is the same as Eq. (52), except that the static ρ correlation function decays monotonically. For $\gamma=0$ in Eq. (34), a simple scaling analysis shows immediately that (i) the contribution of the ρ fluctuations to the viscosity varies *linearly* with the correlation length ξ_ρ [28], and (ii) that the characteristic frequency $\omega^*_{v,\rho}$ of this contribution scales as $\omega^*_{v,\rho} \sim \xi_\rho^{-4}$. We want to emphasize that, since ξ_ρ never gets very large in a microemulsion or sponge phase, the contribution of the ρ fluctuations to the viscosity is much smaller than the Φ contributions for $\omega < \omega_v^*$. However, for $\omega_v^* \ll \omega \ll \omega^*_{v,\rho}$ it leads to an approximately frequency-independent value of the viscosity, which depends on the amphiphile fluctuations.

Finally, we want to mention that on the one-loop level of the calculation of the self-energy, the viscosity η does not contain contributions due to hydrodynamic interactions. This corresponds to Rouse dynamics in polymer systems. The effect of hydrodynamic interactions on $\eta(\omega)$ appears first in a two-loop approximation of the self-energy.

V. SOUND ATTENUATION AND DISPERSION

A comparison of Eq. (43) for the viscosity with Eqs. (49) and (50) for the sound velocity and sound damping shows immediately the strong similarity of these quantities, except that in the case of sound the self-energy $\Sigma_{\mathbf{j}_L\tilde{\mathbf{j}}_L}(\mathbf{k},\omega)$ appears, which involves the longitudinal rather than the transverse momentum density.

The leading contribution to the self-energy $\Sigma_{\mathbf{j}_L\tilde{\mathbf{j}}_L}(\mathbf{k},\omega)$ is the Feynman diagram shown in Fig. 5. The expressions for the propagators and vertices listed in Appendix A give the explicit result

$$\Sigma_{\mathbf{j}_L\tilde{\mathbf{j}}_L}(\mathbf{k},\omega) = g_0^2 \int \frac{d^3p}{(2\pi)^3} \frac{\mathbf{p}\cdot\mathcal{L}_k}{\chi_0^{-1}(\mathbf{p}-\mathbf{k}) - i\omega + \Gamma_\Phi p^2 \chi_0^{-1}(p) + \Gamma_\Phi (\mathbf{p}-\mathbf{k})^2 \chi_0^{-1}(\mathbf{p}-\mathbf{k})} \frac{\mathcal{L}_k\cdot[(\mathbf{p}-\mathbf{k})\chi_0^{-1}(\mathbf{p}-\mathbf{k}) - \mathbf{p}\chi_0^{-1}(p)]}{}, \tag{66}$$

where $[\mathcal{L}_k]_{\alpha\beta} = k_\alpha k_\beta / k^2$ is the longitudinal projector (so that $\mathcal{L}_k \cdot \mathbf{k} = \mathbf{k}$). In Eq. (66), the integral over the internal frequency ω' has already been carried out. From Eq. (66), one obtains

$$\begin{aligned}\gamma_{\mathbf{j}_L\tilde{\mathbf{j}}_L}(\omega) = \frac{g_0^2}{15\pi^2} \int_0^\infty dp \frac{p^4}{\chi_0^{-1}(p)[-i\omega + 2\Gamma_\Phi p^2 \chi_0^{-1}(p)]} \\ \times \Bigg\{ (15 b_0 + 42 c p^2) \\ + \frac{12 h(p) p^2 + 5\chi_0^{-1}(p)}{\chi_0^{-1}(p)[-i\omega + 2\Gamma_\Phi p^2 \chi_0^{-1}(p)]} \\ \times [i 2 h(p)\omega - \Gamma_\Phi \chi_0^{-1}(p)(6 h(p) p^2 \\ + \chi_0^{-1}(p))] \Bigg\}.\end{aligned} \tag{67}$$

Instead of the sound velocity and damping, sound data are often plotted as normalized dispersion

$$\Delta(\omega) \equiv 1 - \frac{c^2(0)}{c^2(\omega)} \tag{68}$$

and attenuation per wavelength

$$\alpha_\lambda(\omega) \equiv \frac{\pi\omega}{c^2(\omega)} [D(\omega) - D_\infty], \tag{69}$$

or $\alpha_\lambda(\omega)/c^2(\omega)$ [63,48,37]. Typical curves for $\Delta(\omega)$ and $\alpha_\lambda(\omega)/c^2(\omega)$ are shown in Figs. 6 and 7, respectively. In these figures, the correlation length ξ is varied at fixed domain size $2\pi/q$. For small correlation lengths, the attenuation curve is dominated by a single large peak, very similar to the behavior seen in the vicinity of a critical point [63,48]. For larger ξ, a second peak develops at lower frequencies; the height of this peak increases with increasing ξ, while its position moves to smaller values of ω. The dependence of the peak position and peak height on the domain size $2\pi/q$, on the other hand, is rather weak. The behavior of the dispersion is found to be very similar, where a pronounced shoulder is observed at the characteristic frequency of the attenuation peak.

The results for the viscosity discussed in Sec. IV now indicate that not the dispersion $\Delta(\omega)$ and the attenuation per wavelength $\alpha_\lambda(\omega)$ should have a scaling form, but rather the quantities [64]

$$-\gamma'_{\mathbf{j}_L\tilde{\mathbf{j}}_L}(\omega) = D(\omega) - D_\infty, \tag{70}$$

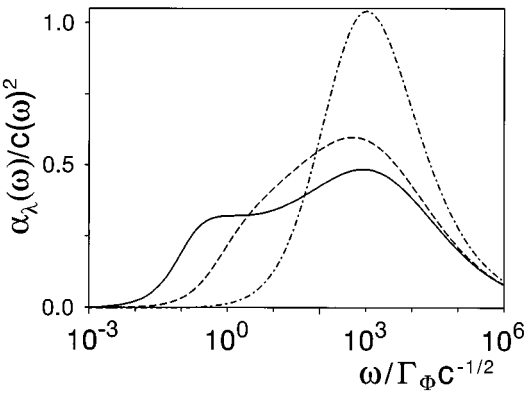

FIG. 7. Sound attenuation $\alpha_\lambda(\omega)/c^2(\omega)$ for $q=0.95$ and $\xi=1.0$ (dashed-dotted line), $\xi=5.0$ (dashed line), $\xi=11.0$ (full line). The parameters are $c=1$, $g_0=1$, and $\lambda_0=1$.

$$-\gamma''_{\mathbf{j}_L\tilde{\mathbf{j}}_L}(\omega)=\frac{c^2(\omega)-c^2(0)}{\omega}, \tag{71}$$

where $D_\infty=\lim_{\omega\to\infty}D(\omega)$. A typical result for the frequency dependence of the self-energy contribution $\gamma_{\mathbf{j}_L\tilde{\mathbf{j}}_L}(\omega)$ for a strongly structured microemulsion indeed looks strikingly similar to the complex viscosity shown in Fig. 2 .

A more detailed analysis of Eq. (66) shows that $\gamma_{\mathbf{j}_L\tilde{\mathbf{j}}_L}(\omega)$ can be written in the scaling form

$$-\gamma_{\mathbf{j}_L\tilde{\mathbf{j}}_L}=\frac{g_0^2}{\Gamma_\Phi c^{1/4}}\overline{\xi^3}S\left(q\xi,\frac{\omega}{\omega_s^*}\right). \tag{72}$$

The characteristic frequency ω_s^*, which is defined by the position of the maximum of $-\gamma''_{\mathbf{j}_L\tilde{\mathbf{j}}_L}$, also has a scaling form [compare Eq. (57)],

$$\omega_s^*=(\Gamma_\Phi c^{-1/2})\overline{\xi^{-6}}\Omega_s(q\xi). \tag{73}$$

The discussion of the scaling behavior of the sound modes now follows closely the discussion in Sec. IV for the viscosity. In the case $\omega=0$, the scaling function S of Eq. (72) can again be calculated analytically,

$$S(y,\omega=0)=\frac{31}{960\pi}\,\frac{1+\frac{3}{62}y^2}{1+y^2}. \tag{74}$$

The scaling function $\Omega_s(q\xi)$ of the characteristic frequency ω_s^* shows the same behavior as the scaling function $\Omega_v(q\xi)$ of the viscosity, compare Fig. 3. The scaling function for the sound modes is well fitted by the expression

$$\Omega_s(q\xi)=5[1+6(q\xi)^2+7(q\xi)^4] \tag{75}$$

over the whole range of the argument. This result indicates that for strongly structured microemulsions with $q\xi\geqslant 5$ the same structural relaxation processes are responsible for both viscoelastic behavior and sound attenuation.

The full scaling function $S(q\xi,\omega/\omega_s^*)$ has to be calculated numerically; its real and imaginary parts are shown in Fig. 8. The asymptotic behavior for small ω is found analytically to be

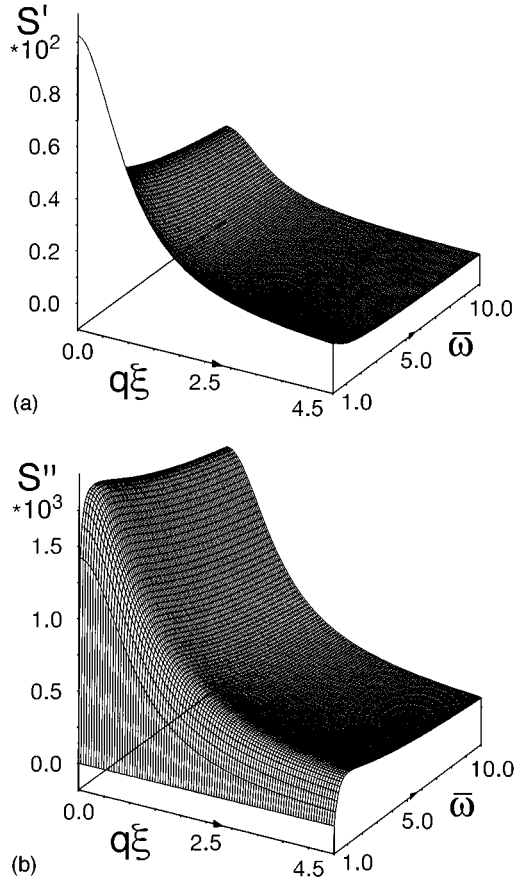

FIG. 8. (a) Real and (b) imaginary part of the scaling function $S(q\xi,\bar{\omega})$ of sound velocity and damping, with $\bar{\omega}=\omega/\omega_s^*$

$$\left.\begin{aligned}\mathrm{Re}[S(\cdot,0)-S(\cdot,\bar{\omega})]&\sim\bar{\omega}^{1/2}\\ \mathrm{Im}[S(\cdot,\bar{\omega})]&\sim\bar{\omega}^{1/2}\end{aligned}\right\}\ \bar{\omega}\to 0, \tag{76}$$

while the asymptotic behavior for large ω is obtained numerically,

$$S(\cdot,\bar{\omega})\sim\bar{\omega}^{-1/2},\quad \bar{\omega}\to\infty. \tag{77}$$

A comparison of Eqs. (76) and (77) with Eqs. (60) and (65) shows that while the large-ω behaviors of the two scaling functions S and V are the same, their small-ω asymptotics are different.

Our results for the scaling form of $\gamma_{\mathbf{j}_L\tilde{\mathbf{j}}_L}(\omega)$ can now be used to discuss the behavior of sound attenuation and dispersion, see Figs. 6 and 7. The dispersion

$$\Delta(\omega)=\frac{-\omega\gamma''_{\mathbf{j}_L\tilde{\mathbf{j}}_L}(\omega)}{\lambda_0^2-\omega\gamma''_{\mathbf{j}_L\tilde{\mathbf{j}}_L}(\omega)} \tag{78}$$

depends only on the imaginary part of $\gamma_{\mathbf{j}_L\tilde{\mathbf{j}}_L}$. Equation (76) therefore implies that $\Delta(\omega)\sim\omega^{3/2}$ for small ω [65]. The self-energy contribution $-\gamma''_{\mathbf{j}_L\tilde{\mathbf{j}}_L}(\omega)$ has a maximum for

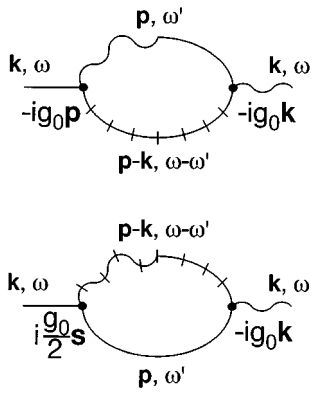

FIG. 9. Feynman diagrams for the self-energy $\Sigma_{\Phi\tilde{\Phi}}(\mathbf{k},\omega)$ in a one-loop approximation. The notation for the various propagators and vertices is explained in Appendix A. The contribution of the left vertex of the second diagram contains the vector $\mathbf{s}=\mathbf{p}\chi_0^{-1}(p)-\mathbf{k}\chi_0^{-1}(k)$.

$\omega=\omega_s^*$, compare Fig. 2, which leads to the shoulder in $\Delta(\omega)$ at approximately the same frequency. Finally, for large ω, Eq. (77) yields $-\omega\gamma''_{\mathbf{j}_L\tilde{\mathbf{j}}_L}(\omega)\sim\omega^{1/2}$, so that $\Delta(\omega)\to 1$. The sound attenuation per wavelength [divided by $c^2(\omega)$],

$$\frac{\alpha_\lambda(\omega)}{c^2(\omega)}=\frac{-\pi\omega\gamma'_{\mathbf{j}_L\tilde{\mathbf{j}}_L}(\omega)}{[\lambda_0^2-\omega\gamma''_{\mathbf{j}_L\tilde{\mathbf{j}}_L}(\omega)]^2}, \tag{79}$$

depends both on the real and imaginary parts of $\gamma_{\mathbf{j}_L\tilde{\mathbf{j}}_L}$. The real part approaches a constant for small ω, so that $\alpha_\lambda(\omega)/c^2(\omega)\sim\omega$ for $\omega\to 0$. The maximum of $-\gamma''_{\mathbf{j}_L\tilde{\mathbf{j}}_L}(\omega)$ and the sharp drop of $-\gamma'_{\mathbf{j}_L\tilde{\mathbf{j}}_L}(\omega)$ at the characteristic frequency ω_s^* lead to the low-frequency peak of the sound attenuation per wavelength. The second peak at higher frequencies occurs — for sufficiently small ω_s^* — in a ω regime, where $\gamma_{\mathbf{j}_L\tilde{\mathbf{j}}_L}(\omega)$ is well approximated by the asymptotic power law (77). Therefore, it is easy to see that a peak occurs at $\omega\sim\lambda_0^4$; with increasing $q\xi$, the position of this peak shifts to larger values of ω [29]. Finally, at very high frequencies, $\alpha_\lambda(\omega)/c^2(\omega)$ decreases as $\omega^{-1/2}$.

VI. DYNAMIC SCATTERING INTENSITY IN BULK CONTRAST

We have shown in Sec. III that the scattering intensity in bulk contrast $G_{\Phi\Phi}(\mathbf{k},\omega)$ is given by Eq. (38). We calculate the self-energy here for model H, i.e., we take the fluid to be incompressible. The two Feynman diagrams, which contribute to $\Sigma_{\Phi\tilde{\Phi}}(\mathbf{k},\omega)$ in this case in a one-loop approximation are shown in Fig. 9. The expressions for the propagators and vertices given in Appendix A imply

$$\Sigma_{\Phi\tilde{\Phi}}(\mathbf{k},\omega)=-g_0^2\int\frac{d^3p}{(2\pi)^3}\frac{\chi_0(p)}{\chi_0(k)}\times\frac{\mathbf{k}\cdot\mathcal{T}_{p-k}\cdot\mathbf{k}}{-i\omega+\Gamma_T(\mathbf{p}-\mathbf{k})^2+\Gamma_\Phi p^m\chi_0^{-1}(p)}. \tag{80}$$

The expression (38) together with (80) for $G_{\Phi\Phi}(\mathbf{k},\omega)$ has been analyzed in detail in Refs. [24,25] as a function of ω; the intermediate scattering function $G_{\Phi\Phi}(\mathbf{k},t)$ as a function of time t was calculated by a numerical Fourier transformation.

Unfortunately, it is very difficult to extract the asymptotic behavior of the scattering intensity for short and large times t from Eq. (38). This is much easier when the perturbation theory is formulated directly for $G_{\Phi\Phi}(\mathbf{k},t)$. The Dyson equation reads in this case

$$G(\mathbf{k},t)=G^{(0)}(\mathbf{k},t)+\int_{-\infty}^{\infty}dt_1\int_{-\infty}^{\infty}dt_2G^{(0)}(\mathbf{k},t-t_1)\times\Sigma(\mathbf{k},t_1-t_2)G(\mathbf{k},t_2) \tag{81}$$

for the *matrix* $G(\mathbf{k},t)$ of correlation and response functions. In the form (81), the Dyson equation cannot be solved for the full correlation matrix $G(\mathbf{k},t)$. Therefore, we calculate the correlation function in the first Born approximation, i.e., we replace the full correlation matrix on the rhs of Eq. (81) by the bare correlation matrix $G^{(0)}(\mathbf{k},t)$. In this case, one finds

$$G_{\Phi\Phi}(\mathbf{k},t)=G^{(0)}_{\Phi\Phi}(\mathbf{k},t)+\Sigma_\Phi(\mathbf{k},t), \tag{82}$$

with

$$\Sigma_\Phi(t)=\int_{-\infty}^{\infty}dt_1\int_{-\infty}^{\infty}dt_2[G^{(0)}_{\tilde{\Phi}\Phi}(t_1-t)\Sigma_{\tilde{\Phi}\tilde{\Phi}}(t_1-t_2)G^{(0)}_{\tilde{\Phi}\Phi}(t_2)+G^{(0)}_{\tilde{\Phi}\Phi}(t_1-t)\Sigma_{\Phi\tilde{\Phi}}(t_2-t_1)G^{(0)}_{\Phi\Phi}(t_2)+G^{(0)}_{\Phi\Phi}(t-t_1)\Sigma_{\Phi\tilde{\Phi}}(t_1-t_2)G^{(0)}_{\tilde{\Phi}\Phi}(t_2)], \tag{83}$$

where the argument $\mathbf{k}$ has been suppressed for simplicity. The bare propagators are obtained easily by a Fourier transformation from the ω functions listed in Appendix A; in particular, the propagators, which appear in Eqs. (82) and (83), are found to be

$$G^{(0)}_{\tilde{\Phi}\Phi}(\mathbf{k},t)=\exp[-\Gamma_\Phi k^m\chi_0^{-1}(k)t]\theta(t), \tag{84}$$

$$G^{(0)}_{\Phi\Phi}(\mathbf{k},t)=\chi_0(k)\exp[-\Gamma_\Phi k^m\chi_0^{-1}(k)|t|]. \tag{85}$$

The self-energy of Eq. (83) can be calculated in two different ways, either by a Fourier transformation from Eq. (80), or by an evaluation of the Feynman diagrams of Fig. 9 in t space. Both calculations lead to the remarkably simple result

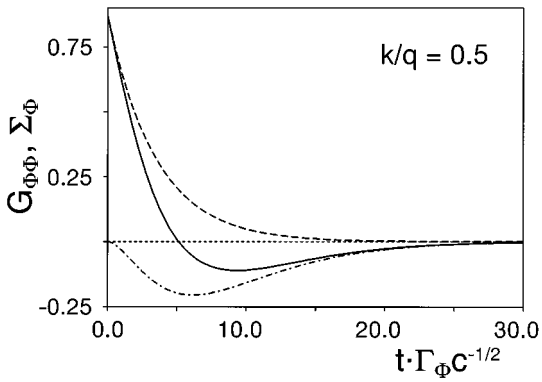

FIG. 10. Dynamic correlation function $G_{\Phi\Phi}(\mathbf{k},t)$ as a function of the scaled time variable $t\Gamma_\Phi c^{-1/2}$ for fixed wave vector $k/q=0.5$. Van-Hove result (dashed line), first Born approximation (full line) and the self-energy contribution $\Sigma_\Phi(\mathbf{k},t)$ are shown. The parameters are $m=2$, $g_0=2$, $\Gamma_\Phi=1$, $\Gamma_T/\Gamma_\Phi=0.3$, $c=1$, $b_0=-1.95$, and $r_2=1$ (so that $q\xi\simeq 8.9$).

$$\Sigma_{\Phi\tilde{\Phi}}(\mathbf{k},t)=-g_0^2\int\frac{d^3p}{(2\pi)^3}\frac{\chi_0(p)}{\chi_0(k)}\mathbf{k}\cdot\mathcal{T}_{p-k}\cdot\mathbf{k}\times\exp\{-[\Gamma_T(\mathbf{p}-\mathbf{k})^2+\Gamma_\Phi p^m\chi_0^{-1}(p)]t\}\theta(t). \tag{86}$$

The second self-energy term is again obtained from the fluctuation-dissipation theorem,

$$\Sigma_{\tilde{\Phi}\tilde{\Phi}}(\mathbf{k},t)=-\chi_0(k)[\Sigma_{\Phi\tilde{\Phi}}(\mathbf{k},t)+\Sigma_{\Phi\tilde{\Phi}}(\mathbf{k},-t)]. \tag{87}$$

The insertion of these results into Eq. (83), and the subsequent integration over the internal times t_1 and t_2 finally yields

$$\Sigma_\Phi(\mathbf{k},t)=g_0^2\int\frac{d^3p}{(2\pi)^3}\chi_0(p)\mathbf{k}\cdot\mathcal{T}_{p-k}\cdot\mathbf{k}\times\left\{\frac{1}{\nu(\mathbf{k})-\mu(\mathbf{p},\mathbf{k})}\left[\frac{1}{\nu(\mathbf{k})-\mu(\mathbf{p},\mathbf{k})}+t\right]e^{-\nu(\mathbf{k})t}-\frac{1}{[\nu(\mathbf{k})-\mu(\mathbf{p},\mathbf{k})]^2}e^{-\mu(\mathbf{p},\mathbf{k})t}\right\}, \tag{88}$$

with

$$\nu(\mathbf{k})\equiv\Gamma_\Phi k^m\chi_0^{-1}(k), \tag{89}$$

$$\mu(\mathbf{p},\mathbf{k})\equiv\Gamma_T(\mathbf{p}-\mathbf{k})^2+\Gamma_\Phi p^m\chi_0^{-1}(p). \tag{90}$$

The remaining integral over the internal wave vector $\mathbf{p}$ in Eq. (88) has to be evaluated numerically; note that the apparent singularity of the integrand cancels out.

A typical result for the time dependence of the dynamic scattering intensity $G_{\Phi\Phi}(\mathbf{k},t)$ for small solvent viscosity Γ_T is shown in Fig. 10. The first Born approximation gives an overshoot at intermediate times, followed by a monotonic exponential decay at large times.

Let us first consider the behavior of the correlation function for short times t. In this limit, the self-energy contribution is given by

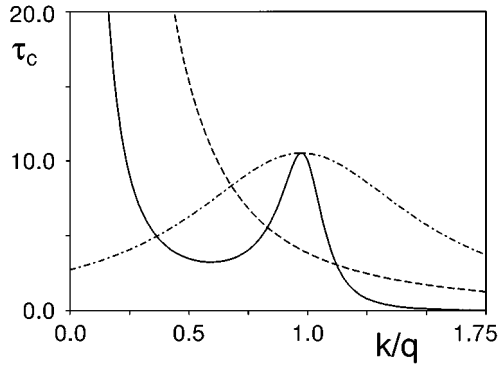

FIG. 11. Relaxation times $\tau_c^{(1)}(k)$ (solid line), $\tau_c^{(2)}(k)$ (dashed line) and $\tau_c^{(3)}(k)$ (dashed-dotted line) of the dynamic scattering intensity for a strongly structured microemulsion. The parameters are $m=2$, $\Gamma_\Phi=1$, $\Gamma_T/\Gamma_\Phi=0.3$, $c=1$, $b_0=-1.95$, and $r_2=1$ (so that $q\xi\simeq 8.9$).

$$\Sigma_\Phi(\mathbf{k},t)=-\frac{g_0^2}{2}\left[\int\frac{d^3p}{(2\pi)^3}\frac{\mathbf{k}\cdot\mathcal{T}_{\mathbf{p}-\mathbf{k}}\cdot\mathbf{k}}{\chi_0^{-1}(p)}\right]t^2+O(t^3), \tag{91}$$

while the Gaussian correlation function decays as

$$G_{\Phi\Phi}^{(0)}(\mathbf{k},t)=\chi_0(k)[1-\Gamma_\Phi k^m\chi_0^{-1}(k)t+O(t^2)]. \tag{92}$$

Thus the short-time behavior of the dynamic scattering intensity remains unchanged by hydrodynamic modes.

The analysis of the asymptotic behavior for large t is more complicated. The integral (88) has to be evaluated by the saddle-point method [66] in this case. A lengthy and somewhat tedious calculation yields

$$G_{\Phi\Phi}(\mathbf{k},t)\propto t^{-5/2}\exp[-t/\tau_c(k)], \tag{93}$$

i.e., an exponential decay with a relaxation time $\tau_c(k)$, together with an *algebraic* prefactor. The relaxation time is given by $\tau_c(k)=\max[\tau_c^{(1)}(k),\tau_c^{(2)}(k),\tau_c^{(3)}(k)]$, where

$$\tau_c^{(1)}(k)=\frac{1}{\Gamma_\Phi k^m\chi_0^{-1}(k)}, \tag{94}$$

$$\tau_c^{(2)}(k)=\frac{1}{\Gamma_T(p_<-k)^2+\Gamma_\Phi p_<^m\chi_0^{-1}(p_<)}, \tag{95}$$

$$\tau_c^{(3)}(k)=\frac{1}{\Gamma_T(\overline{p}-k)^2+\Gamma_\Phi\overline{p}^m\chi_0^{-1}(\overline{p})}. \tag{96}$$

The wave vectors $p_<$ and $\overline{p}$, which appear in Eqs. (95) and (96), are determined to sufficient accuracy by $p_<=k\Gamma_T/(\Gamma_T+2\Gamma_\Phi r_2)+O(k^3)$ and $\overline{p}=\overline{q}+a_1(k-\overline{q})+O[(k-\overline{q})^2]$, where $\overline{q}^2=(-b_0+\sqrt{b_0^2-3cr_2})/3c$ and $a_1^{-1}=1+2(15c\overline{q}^4+6b_0\overline{q}^2+r_2)\Gamma_\Phi/\Gamma_T$. The dependence of these relaxation times on the wave vector k is shown in Fig. 11 for $m=2$. For small k, the relaxation time $\tau_c(k)$ diverges as k^{-2}, compare Eq. (94), due to the conservation of the order parameter. Note that this divergence implies that the decay of the correlation function for $k\equiv 0$ is *purely algebraic*. The internal structure of the microemulsion is re-

flected in a maximum of the $\tau_c(k)$ at $k \simeq q$. Finally, the relaxation time decreases rapidly for large k.

The relaxation times shown in Fig. 11 are calculated for a strongly structured microemulsion ($q\xi \simeq 8.9$), with a small solvent viscosity Γ_T. With increasing Γ_T, the width of the peak of $\tau_c^{(3)}(k)$ narrows; simultaneously, the function $\tau_c^{(2)}(k)$ decreases in magnitude, and approaches $\tau_c^{(1)}(k)$ for small k. Finally, for $\Gamma_T/\Gamma_\Phi \gg 1$, $\tau_c(k) = \tau_c^{(1)}(k)$. With decreasing $q\xi$, on the other hand, the maximum of the relaxation time at $k=q$ decreases, and disappears at $q\xi \simeq 3.5$. For smaller $q\xi < 3.5$, $\tau_c(k)$ is a monotonically decreasing function of k, with $\tau_c(k) \equiv \tau_c^{(2)}(k)$ for all wave vectors.

VII. DYNAMIC SCATTERING INTENSITY IN FILM CONTRAST

The dynamic scattering intensity in film contrast, $G_{\rho\rho}(\mathbf{k},\omega)$, is given by Eq. (39). The Feynman diagrams, which contribute to $\Sigma_{\rho\tilde{\rho}}(\mathbf{k},\omega)$ to one-loop order, are shown in Fig. 12. The two diagrams on the lhs of Fig. 12 are completely analogous to the diagrams of Fig. 9 for the self-energy $\Sigma_{\Phi\tilde{\Phi}}(\mathbf{k},\omega)$, and describe the coupling of the amphiphile density to the hydrodynamic variables. The diagram on the rhs of Fig. 12, on the other hand, describes the coupling of the amphiphile density to the fluctuations of the order parameter Φ; note that the strength of the vertices is determined by dissipative coupling constants in this case, while all previous diagrams contained mode-coupling coefficients as vertex strengths. Therefore, it is natural to write $\Sigma_{\rho\tilde{\rho}}(\mathbf{k},\omega)$ as a sum of two contributions,

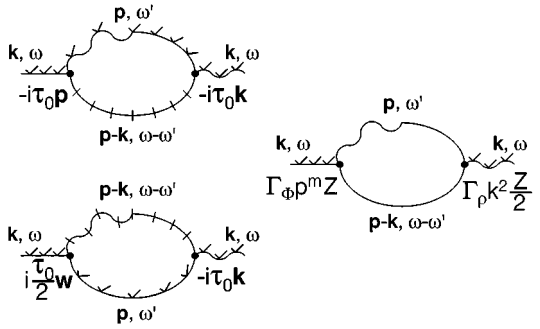

FIG. 12. Feynman diagrams for the self-energy $\Sigma_{\rho\tilde{\rho}}(\mathbf{k},\omega)$ in a one-loop approximation. The notation for the various propagators and vertices is explained in Appendix A. The vertices contain the contributions $\mathbf{w} = \mathbf{p}\chi_\rho^{-1}(p) - \mathbf{k}\chi_\rho^{-1}(k)$ and $Z = 2\beta_1 - 2\beta_2 k^2 - \beta_3 p^2 - \beta_3(\mathbf{p}-\mathbf{k})^2$.

$$\Sigma_{\rho\tilde{\rho}}(\mathbf{k},\omega) \equiv \Sigma_{\rho\tilde{\rho}}^{(H)}(\mathbf{k},\omega) + \Sigma_{\rho\tilde{\rho}}^{(C)}(\mathbf{k},\omega), \tag{97}$$

where the hydrodynamic part [compare Eq. (80)] is given by

$$\Sigma_{\rho\tilde{\rho}}^{(H)}(\mathbf{k},\omega) = -\tau_0^2 \int \frac{d^3p}{(2\pi)^3} \frac{\chi_\rho(p)}{\chi_\rho(k)} \times \frac{\mathbf{k}\cdot\mathcal{T}_{p-k}\cdot\mathbf{k}}{-i\omega + \Gamma_T(\mathbf{p}-\mathbf{k})^2 + \Gamma_\rho p^2 \chi_\rho^{-1}(p)}, \tag{98}$$

and the order-parameter part by

$$\Sigma_{\rho\tilde{\rho}}^{(C)}(\mathbf{k},\omega) = \Gamma_\rho \Gamma_\Phi k^2 \int \frac{d^3p}{(2\pi)^3} \frac{p^m}{\chi_0^{-1}(\mathbf{p}-\mathbf{k})} \frac{[2\beta_1 - 2\beta_2 k^2 - \beta_3 p^2 - \beta_3(\mathbf{p}-\mathbf{k})^2]^2}{-i\omega + \Gamma_\Phi p^m \chi_0^{-1}(p) + \Gamma_\Phi (\mathbf{p}-\mathbf{k})^m \chi_0^{-1}(\mathbf{p}-\mathbf{k})}. \tag{99}$$

The advantage of this separation is that the effects of the hydrodynamic modes (model H) and of coupling to the order-parameter fluctuations (model C) on $G_{\rho\rho}(\mathbf{k},\omega)$ can be discussed independently.

The self-energy contribution $\Sigma_{\tilde{\rho}\tilde{\rho}}(\mathbf{k},\omega)$ in Eq. (39) can again be obtained from the fluctuation-dissipation theorem, which reads in this case (see Appendix B for details)

$$\Sigma_{\tilde{\rho}\tilde{\rho}}^{(H)}(\mathbf{k},\omega) = -2\chi_\rho(k)\,\mathrm{Re}\{\Sigma_{\rho\tilde{\rho}}^{(H)}(\mathbf{k},\omega)\}, \tag{100}$$

$$\Sigma_{\tilde{\rho}\tilde{\rho}}^{(C)}(\mathbf{k},\omega) = \frac{2\Gamma_\rho k^2}{\omega}\,\mathrm{Im}\{\Sigma_{\rho\tilde{\rho}}^{(C)}(\mathbf{k},\omega)\}. \tag{101}$$

The dynamic scattering intensity in film contrast $G_{\rho\rho}(\mathbf{k},\omega)$ is shown in Figs. 13 and 14 as a function of ω for $k=q$, and as a function of k for fixed ω, respectively. These curves demonstrate several properties of $G_{\rho\rho}(\mathbf{k},\omega)$. First, note that the effect of the conservation of the order parameter Φ on the amphiphile scattering intensity is rather weak; the curves for $m=2$ and $m=0$ almost coincide. Second, the dynamic correlation function vanishes for $\omega \neq 0$ as k^2 for $k \to 0$ as a consequence of the conservation of the amphiphile concentration. Third, the main contribution to the one-loop self-energy $\Sigma_{\rho\tilde{\rho}}(\mathbf{k},\omega)$ arises from the coupling to the order parameter Φ, while the effect of hydrodynamic relaxation modes would be difficult to distinguish in the scattering curves of Figs. 13 and 14. Finally, the *full* dynamic correlation function at fixed wave vector k satisfies the (exact) sum rule [47]

$$\int_{-\infty}^{\infty} \frac{d\omega}{2\pi} G_{\rho\rho}(\mathbf{k},\omega) = G_{\rho\rho}^{(stat)}(\mathbf{k}). \tag{102}$$

We find that our one-loop results fulfill this condition very well; calculations for several wave vectors k showed deviations of less than one percent.

In order to extract the asymptotic behavior of the intermediate correlation function, $G_{\rho\rho}(\mathbf{k},t)$, for short and long times

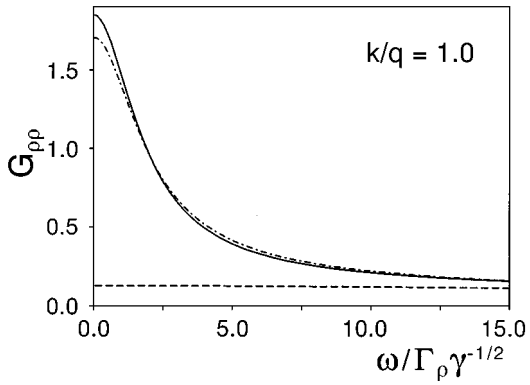

FIG. 13. Dynamic scattering intensity $G_{\rho\rho}(\mathbf{k},\omega)$ in film contrast with $k=q$ as a function of the scaled frequency $\omega/(\Gamma_\rho\gamma^{-1/2})$, for both conserved (full line) and nonconserved (dashed-dotted line) order parameter Φ. The van-Hove approximation is also shown (dashed line). The parameters are $\tau_0=2$, $\Gamma_\rho=1$, $\Gamma_\Phi=1$, $\Gamma_T=1$, $\beta_1=0.7$, $\beta_2=-1.0$, $\beta_3=-0.1$, $\alpha=1$, $\beta=1$, $\gamma=0.01$, $c=1$, $b_0=-1.95$, and $r_2=1$.

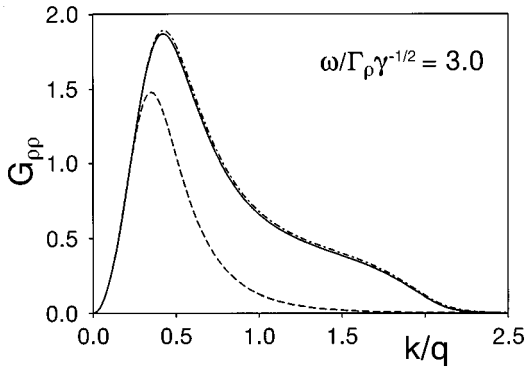

FIG. 14. Dynamic scattering intensity $G_{\rho\rho}(\mathbf{k},\omega)$ in film contrast with $\omega/(\Gamma_\rho\gamma^{-1/2})=3.0$ as a function of the scaled wave vector k/q, for both conserved (full line) and nonconserved (dashed-dotted line) order parameter Φ. The van-Hove approximation is also shown (dashed line). The parameters are $\tau_0=2$, $\Gamma_\rho=1$, $\Gamma_\Phi=1$, $\Gamma_T=1$, $\beta_1=0.7$, $\beta_2=-1.0$, $\beta_3=-0.1$, $\alpha=1$, $\beta=1$, $\gamma=0.01$, $c=1$, $b_0=-1.95$, and $r_2=1$.

t, we follow again the route taken in Sec. VI. In the first Born approximation, the correlation function then reads

$$G_{\rho\rho}(\mathbf{k},t)=G^{(0)}_{\rho\rho}(\mathbf{k},t)+\Sigma_\rho(\mathbf{k},t), \tag{103}$$

where

$$G^{(0)}_{\rho\rho}(\mathbf{k},t)=\chi_\rho(k)\exp[-\Gamma_\rho k^2\chi_\rho^{-1}(k)|t|], \tag{104}$$

and $\Sigma_\rho(\mathbf{k},t)$ is given by an expression completely analogous to Eq. (83), with Φ and $\tilde{\Phi}$ replaced by ρ and $\tilde{\rho}$, respectively. We divide the self-energy terms again into a hydrodynamic part, and a part describing the coupling to the order parameter fluctuations. The latter contribution — obtained by a Fourier transformation from Eqs. (99) and (101) — is given by

$$\begin{aligned}\Sigma^{(C)}_{\rho\tilde{\rho}}(\mathbf{k},t)=&\frac{1}{2}\Gamma_\rho^2k^4\int\frac{d^3p}{(2\pi)^3}\\&\times\frac{[2\beta_1-2\beta_2k^2-\beta_3p^2-\beta_3(\mathbf{p}-\mathbf{k})^2]^2}{\chi_0^{-1}(\mathbf{p}-\mathbf{k})\chi_0^{-1}(p)}\\&\times\exp\{-\Gamma_\Phi[(\mathbf{p}-\mathbf{k})^m\chi_0^{-1}(\mathbf{p}-\mathbf{k})\\&+p^m\chi_0^{-1}(p)]|t|\}.\end{aligned} \tag{105}$$

The self-energy $\Sigma^{(C)}_{\rho\tilde{\rho}}(\mathbf{k},t)$ follows from the fluctuation-dissipation theorem, which reads in this case

$$\frac{\partial}{\partial t}\Sigma^{(C)}_{\tilde{\rho}\rho}(\mathbf{k},t)=-\Gamma_\rho k^2[\Sigma^{(C)}_{\rho\tilde{\rho}}(\mathbf{k},t)+\Sigma^{(C)}_{\rho\tilde{\rho}}(\mathbf{k},-t)], \tag{106}$$

together with $\Sigma^{(C)}_{\rho\tilde{\rho}}(\mathbf{k},t)\sim\theta(t)$. These expressions can then be inserted back into the analog of Eq. (83); an integration over the internal time variables t_1 and t_2 finally yields

$$\begin{aligned}\Sigma^{(C)}_{\rho}(\mathbf{k},t)=&\frac{1}{2}\Gamma_\rho^2k^4\int\frac{d^3p}{(2\pi)^3}\\&\times\frac{[2\beta_1-2\beta_2k^2-\beta_3p^2-\beta_3(\mathbf{p}-\mathbf{k})^2]^2}{\chi_0^{-1}(\mathbf{p}-\mathbf{k})\chi_0^{-1}(p)}\\&\times\left\{\frac{\lambda(\mathbf{p},\mathbf{k})}{\kappa(\mathbf{k})[\kappa(\mathbf{k})-\lambda(\mathbf{p},\mathbf{k})]}\right.\\&\times\left[\frac{\lambda(\mathbf{p},\mathbf{k})-2\kappa(\mathbf{k})}{\kappa(\mathbf{k})[\kappa(\mathbf{k})-\lambda(\mathbf{p},\mathbf{k})]}-t\right]e^{-\kappa(\mathbf{k})t}\\&\left.+\frac{1}{[\kappa(\mathbf{k})-\lambda(\mathbf{p},\mathbf{k})]^2}e^{-\lambda(\mathbf{p},\mathbf{k})t}\right\},\end{aligned} \tag{107}$$

where

$$\kappa(\mathbf{k})\equiv\Gamma_\rho k^2\chi_\rho^{-1}(k), \tag{108}$$

$$\lambda(\mathbf{p},\mathbf{k})\equiv\Gamma_\Phi[(\mathbf{p}-\mathbf{k})^m\chi_0^{-1}(\mathbf{p}-\mathbf{k})+p^m\chi_0^{-1}(p)]. \tag{109}$$

A typical result for the time dependence of the dynamic amphiphile scattering intensity $G_{\rho\rho}(\mathbf{k},t)$ is shown in Fig. 15.

The expression (107) can now be used to extract the asymptotic time behavior of the amphiphile correlation function. For small times t, an expansion of Eq. (107) in powers of t implies

$$\begin{aligned}\Sigma^{(C)}_{\rho}(\mathbf{k},t)=&\Sigma^{stat}_\rho(\mathbf{k})\\&-\frac{1}{12}\Gamma_\rho^2k^4\left[\int\frac{d^3p}{(2\pi)^3}\,\frac{\lambda(\mathbf{p},\mathbf{k})}{\chi_0^{-1}(\mathbf{p}-\mathbf{k})\chi_0^{-1}(p)}\right.\\&\left.\times[2\beta_1-2\beta_2k^2-\beta_3p^2-\beta_3(\mathbf{p}-\mathbf{k})^2]^2\right]t^3\\&+O(t^4),\end{aligned} \tag{110}$$

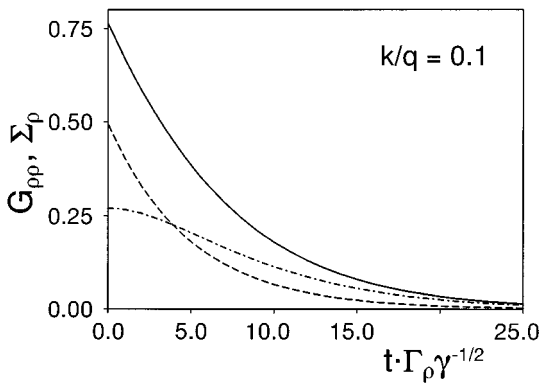

FIG. 15. Dynamic correlation function $G_{\rho\rho}(\mathbf{k},t)$ as a function of the scaled time variable $t\Gamma_\rho\gamma^{-1/2}$ for fixed wave vector $k/q=0.1$ and nonconserved order parameter Φ. Van-Hove result (dashed line), first Born approximation (full line) and the self-energy contribution $\Sigma_\rho(\mathbf{k},t)$ are shown. The parameters are $m=0$, $\tau_0=0$, $\Gamma_\rho=1$, $\Gamma_\Phi=1$, $\Gamma_T=1$, $\beta_1=0.7$, $\beta_2=-1.0$, $\beta_3=-0.1$, $\alpha=1$, $\beta=1$, $\gamma=0.01$, $c=1$, $b_0=-1.95$, and $r_2=1$.

where $\Sigma_\rho^{stat}(\mathbf{k})=\Sigma_\rho^{(C)}(\mathbf{k},t=0)$ is the static self-energy contribution. Therefore, the linear time dependence of the Gaussian correlation function for $t\to 0$,

$$G_{\rho\rho}^{(0)}(\mathbf{k},t)=\chi_\rho(k)[1-\Gamma_\rho k^2\chi_\rho^{-1}(k)t+O(t^2)], \quad (111)$$

remains unchanged, just as for the scattering intensity in bulk contrast, compare Eqs. (91) and (92). Note, however, that the value of $G_{\rho\rho}(\mathbf{k},t=0)$ is modified in this case, since the static self-energy $\Sigma_\rho^{stat}(\mathbf{k})$ is nonzero.

In order to extract the asymptotic behavior of $G_{\rho\rho}(\mathbf{k},t)$ for large times, we employ again the saddle-point method [66]. The analysis is somewhat more complicated than for the correlation function $G_{\Phi\Phi}(\mathbf{k},t)$ in bulk contrast (compare Sec. VI) , since both conserved and nonconserved order parameter Φ has to be considered, and also the limits of small and large amphiphile mobility have to be investigated.

Let us consider first the case of low amphiphile mobility, i.e., $\Gamma_\rho \ll \Gamma_\Phi c^{(2-m)/4}$. We find that in this limit the fluctuations of the order parameter are irrelevant for the long-time behavior of $G_{\rho\rho}(\mathbf{k},t)$. The self-energy $\Sigma_\rho^{(C)}(\mathbf{k},t)$ is dominated by the first exponential in Eq. (107), which leads to

$$G_{\rho\rho}(\mathbf{k},t)\propto t\exp[-t/\theta_c^{(0)}(k)] \quad (\Gamma_\rho \ll \Gamma_\Phi c^{(2-m)/4}), \quad (112)$$

with

$$\theta_c^{(0)}(k)\equiv\frac{1}{\Gamma_\rho k^2\chi_\rho^{-1}(k)}. \quad (113)$$

This result applies both for conserved and for nonconserved order parameter Φ.

In the opposite limit of slow order-parameter dynamics $\Gamma_\rho \geqslant \Gamma_\Phi c^{(2-m)/4}$ the conservation or nonconservation of the order parameter becomes important. In the latter case, i.e., for $m=0$, the intermediate scattering intensity of well-structured microemulsion or sponge phases (with $q\xi>1$) decays for $t\to\infty$ as

$$G_{\rho\rho}(\mathbf{k},t)\propto t^{-1}\exp(-t/\theta_c^{(2)}) \quad (\Gamma_\Phi c^{1/2} \ll \Gamma_\rho, m=0), \quad (114)$$

with a *k-independent* relaxation time

$$\theta_c^{(2)}\equiv\frac{1}{2\Gamma_\Phi\overline{q^m}\chi_0^{-1}(\overline{q})}, \quad (115)$$

where $\overline{q}=(-b_0/2c)^{1/2}$. The investigation of a system with a conserved order parameter Φ, i.e., with $m=2$, turns out to be more complicated, because the exponent $\lambda(\mathbf{p},\mathbf{k})$ of Eqs. (107), (109) has several minima in this case. A somewhat tedious but straightforward calculation shows that there are several different regimes, which have to be distinguished. For a strongly structured microemulsion or sponge phase, with $q\xi>3.5$, we find

$$G_{\rho\rho}(\mathbf{k},t)\propto\begin{cases} t^{-3/2}\exp[-t/\theta_c^{(1)}(k)] & k\ll\xi^{-1} \\ t^{-1}\exp(-t/\theta_c^{(2)}) & \xi^{-1}<k<q \\ t^{-3/2}\exp[-t/\theta_c^{(3)}(k)] & k\approx q \\ t^{-1}\exp(-t/\theta_c^{(2)}) & k>q \end{cases} \quad \text{for}$$

$$(\Gamma_\Phi \ll \Gamma_\rho, m=2). \quad (116)$$

The relaxation time $\theta_c^{(2)}$ is still given by Eq. (115), but with the wave vector $\overline{q}$ now determined by $\overline{q^2}=(-b_0+\sqrt{b_0^2-3cr_2})/3c$ [compare Eq. (96)]. In addition, the relaxation times

$$\theta_c^{(1)}(k)\equiv\frac{1}{2\Gamma_\Phi(k/2)^m\chi_0^{-1}(k/2)} \quad (117)$$

and

$$\theta_c^{(3)}(k)\equiv\frac{1}{\Gamma_\Phi[(\hat{p}-k)^m\chi_0^{-1}(\hat{p}-k)+\hat{p}^m\chi_0^{-1}(\hat{p})]} \quad (118)$$

appear, where

$$\hat{p}=\frac{k}{2}+[-15ck^2-4b_0+2(45c^2k^4+12cb_0k^2+4b_0^2 -12cr_2)^{1/2}]^{1/2}(12c)^{-1/2}. \quad (119)$$

The relaxation times $\theta_c^{(0)}(k)$, $\theta_c^{(1)}(k)$, $\theta_c^{(2)}$ and $\theta_c^{(3)}(k)$ are plotted as a function of the wave vector k for a system with $q\xi\simeq 8.9$ in Fig. 16. The various regimes of Eq. (116) arise from the fact that different relaxation times dominate over some range of wave vectors. Note that $\theta_c^{(1)}(k)$ diverges in the limit $k\to 0$, so that $G_{\rho\rho}(k=0,t)\sim t^{-3/2}$, i.e., the correlation function decays *purely algebraically* in time [27].

In our discussion of the relaxation times, we have so far completely neglected the ''hydrodynamic'' contribution $\Sigma_\rho^{(H)}(\mathbf{k},t)$ of $\Sigma_\rho(\mathbf{k},t)$ in Eq. (103). Due to the completely analogous structure of the dynamic equations for the order parameter and for the amphiphile concentration with respect to the coupling to hydrodynamic variables, the analysis of this term does not require any new calculations. Rather,

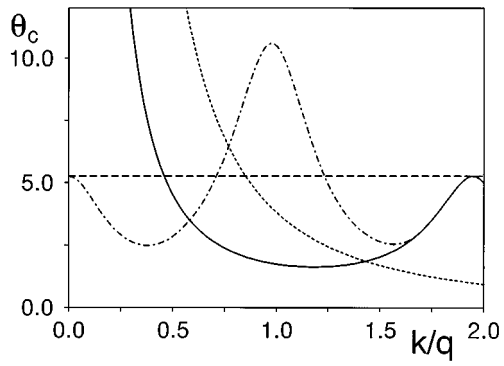

FIG. 16. Asymptotic relaxation times $\theta_c^{(1)}(k)$ (full line), $\theta_c^{(2)}$ (dashed line), $\theta_c^{(3)}(k)$ (dashed-dotted line), together with the hydrodynamic relaxation time $\theta_c^{(4)}(k)$ (dotted line), for conserved order parameter Φ and $\Gamma_\Phi \ll \Gamma_\rho$. The parameters are $\Gamma_\Phi = 1$, $c = 1$, $b_0 = -1.95$, and $r_2 = 1$ (so that $q\xi \simeq 8.9$).

$\Sigma_\rho^{(H)}(\mathbf{k},t)$ is given by Eq. (88), with $\nu(\mathbf{k})$ and $\mu(\mathbf{p},\mathbf{k})$, Eqs. (89) and (90), replaced by $\kappa(\mathbf{k})$, Eq. (108), and

$$\sigma(\mathbf{p},\mathbf{k}) \equiv \Gamma_T(\mathbf{p}-\mathbf{k})^2 + \Gamma_\rho p^2 \chi_\rho^{-1}(p), \tag{120}$$

respectively. The self-energy $\Sigma_\rho(\mathbf{k},t)$ corresponds to the self-energy $\Sigma_\Phi(\mathbf{k},t)$ in the limit of very weakly structured microemulsions, since the static scattering intensity $\chi_\rho(k)$ has a peak at $k=0$, and decays monotonically as a function of the wave vector k. In this case, the results of Sec. VI imply that

$$G_{\rho\rho}(\mathbf{k},t) \propto t^{-5/2} \exp(-t/\theta_c^{(4)}) \tag{121}$$

with the relaxation time

$$\theta_c^{(4)}(k) \equiv \frac{1}{\Gamma_T(p_< - k)^2 + \Gamma_\rho p_<^2 \chi_\rho^{-1}(p_<)}, \tag{122}$$

where $p_< = k\Gamma_T/(\Gamma_T + 2\Gamma_\rho \alpha) + O(k^3)$ [compare Eq. (95)]. This ''hydrodynamic'' relaxation time is also shown in Fig. 16; it demonstrates that the hydrodynamic relaxation mode dominates for small k. The upper boundary of this hydrodynamic regime depends on the viscosity Γ_T of the solvent, and decreases with increasing Γ_T. We want to mention parenthetically that the short-time behavior of $G_{\rho\rho}(\mathbf{k},t)$, given by Eq.(111), is *not* modified by the coupling to the hydrodynamic modes, since $\Sigma_\rho^{(H)}(\mathbf{k},t) \sim t^2$ [compare Eq. (91)].

VIII. SUMMARY AND DISCUSSION

We have calculated in this paper the frequency-dependent (complex) viscosity, the sound velocity and damping and the scattering intensity in bulk and film contrast of microemulsion and sponge phases. Our analysis is based on a Ginzburg-Landau model, which has been demonstrated previously to capture many of the essential static properties of these complex fluids. Our field-theoretic calculation of the dynamical properties has the advantage that the effects of the coupling of various hydrodynamic and concentration modes can be studied systematically. Furthermore, this approach guarantees that important general conditions, like the fluctation-dissipation theorem, are automatically satisfied at every level of a perturbation theory.

The main results of this paper can be summarized as follows.

(1) The real part of the viscosity η is almost frequency independent for small frequencies ω. It drops sharply at a characteristic frequency ω^*, which depends on the correlation length ξ and on the domain size $2\pi/q$ of the fluid. With increasing ξ, ω^* decreases strongly, while the dependence on q is rather weak. The imaginary part of η peaks at $\omega = \omega^*$.

(2) The behavior of the sound velocity and damping is very similar to the behavior of the imaginary and real parts of the viscosity. This holds both for the dependence on frequency and on the structural parameters q and ξ. In particular, the *same* characteristic frequency ω^* appears in both cases.

(3) The short-time behavior of the intermediate scattering intensity $G(\mathbf{k},t)$ both in bulk and film contrast, is linear in time t. Mode-coupling terms do not contribute in this limit.

(4) The behavior of the intermediate scattering intensity for large times is given by an exponential decay together with an *algebraic* prefactor. In the case of the scattering intensity in bulk contrast, the prefactor is $t^{-5/2}$. The scattering intensity in film contrast shows several different k regimes, which are characterized by different algebraic factors.

The time dependence of the intermediate scattering intensity requires some further discussion. We have found that the first Born approximation yields a nonmonotonic behavior of the scattering intensity $G_{\Phi\Phi}(\mathbf{k},t)$ in bulk contrast, but asymptotically a monotonic decay for $t \to \infty$. On the other hand, the numerical Fourier transform of the Dyson equation in Ref. [25] showed a damped *oscillatory* decay for large t. First, note that if the longest relaxation time of the mode-coupling terms is *larger* than the Gaussian relaxation time — which has to be the case if the mode-coupling terms dominate the asymptotic behavior for large t — the first Born approximation strictly speaking breaks down for sufficiently large times, since the ''correction'' term becomes much larger than the ''leading'' Gaussian term. Therefore, the Dyson results are more reliable for $t \to \infty$. On the other hand, due to the exponential decay of the correlation function, the Dyson form of $G_{\Phi\Phi}(\mathbf{k},t)$ gets so small for large t that after a few oscillations it cannot be distingushed from numerical inaccuracies. Therefore, it is also very difficult to prove an oscillatory asymptotic behavior. In any case, we are confident that the *algebraic prefactor* is valid independent of an oscillatory or monotonic decay.

The asymptotic behavior of the intermediate scattering intensity in film contrast $G_{\rho\rho}(\mathbf{k},t)$ has already been studied in detail by Granek and Cates in Ref. [27], based on a time-dependent Ginzburg-Landau theory similar to ours. However, their approach differs from ours in two important aspects: (i) their static film correlation function does not contain a peak or shoulder at $k \simeq 2q$, so that the results can only be compared for $k \ll q$, and (ii) they do not include the hydrodynamic modes into the time-dependent model as additional fields, but rather as a memory term. In the more interesting case of a fast amphiphile relaxation, Granek and Cates [27] find for a nonconserved order parameter that the large-time behavior is given by $G_{\rho\rho}(\mathbf{k},t) \sim t^{-3/2} \exp(-t/\tau)$ for

TABLE I. Response propagators.

(a)	$G^{(0)}_{\tilde{\Phi}\Phi}(\mathbf{k},\omega)$	$\dfrac{1}{-i\omega+\Gamma_\Phi k^m \chi_0^{-1}(k)}$
(b)	$G^{(0)}_{\tilde{\rho}\rho}(\mathbf{k},\omega)$	$\dfrac{1}{-i\omega+\Gamma_\rho k^2 \chi_\rho^{-1}(k)}$
(c)	$G^{(0)}_{\tilde{\mathbf{j}}_T\mathbf{j}_T}(\mathbf{k},\omega)$	$\dfrac{1}{-i\omega+\Gamma_T k^2}$
(d)	$G^{(0)}_{\tilde{\mathbf{j}}_L\mathbf{j}_L}(\mathbf{k},\omega)$	$\dfrac{i\omega-\Gamma_p k^2}{\omega^2-\lambda_0^2k^2-\Gamma_L\Gamma_p k^4+i\omega(\Gamma_L+\Gamma_p)k^2}$
(e)	$G^{(0)}_{\tilde{p}p}(\mathbf{k},\omega)$	$\dfrac{i\omega-\Gamma_L k^2}{\omega^2-\lambda_0^2k^2-\Gamma_L\Gamma_p k^4+i\omega(\Gamma_L+\Gamma_p)k^2}$
(f)	$G^{(0)}_{\tilde{\mathbf{j}}_L p}(\mathbf{k},\omega)$	$\dfrac{-i\lambda_0\mathbf{k}}{\omega^2-\lambda_0^2k^2-\Gamma_L\Gamma_p k^4+i\omega(\Gamma_L+\Gamma_p)k^2}$
(g)	$G^{(0)}_{\tilde{p}\mathbf{j}_L}(\mathbf{k},\omega)$	$\dfrac{-i\lambda_0\mathbf{k}}{\omega^2-\lambda_0^2k^2-\Gamma_L\Gamma_p k^4+i\omega(\Gamma_L+\Gamma_p)k^2}$

with $\chi_0^{-1}(k)=2(ck^4+b_0k^2+r_2)$, $\chi_\rho^{-1}(k)=2(\gamma k^4+\beta k^2+\alpha)$

$k\xi\ll 1$, and by $G_{\rho\rho}(\mathbf{k},t)\sim t^{-1/2}\exp(-t/\tau)$ for $k\xi\gg 1$. For a conserved order parameter, they obtain the large-t behavior $G_{\rho\rho}(\mathbf{k},t)\sim t^{-3/2}$ for $k\xi\ll 1$, and $G_{\rho\rho}(\mathbf{k},t)\sim t^{-1/3}\exp(-t/\tau)$ for $k\xi\gg 1$. The relaxation time τ in these expressions is a function of the wave vector k, and is different for conserved and nonconserved order parameters (see Ref. [27] for details). These results have to be compared with our result (114) for nonconserved, and (116) and (121) for conserved order parameters. While there is agreement about the general form of the scattering intensity — an exponential decay with an algebraic prefactor — the algebraic exponents differ in all cases. Furthermore, while we find a linear short-time dependence of the intermediate scattering intensity, Granek and Cates [27] obtain a cusp singularity with the exponent 1/2 for nonconserved and 1/3 for conserved order parameters.

It would now be interesting to perform a self-consistent calculation of the dynamic behavior of microemulsions and sponge phases. Unfortunately, this will require an enormous numerical effort. Furthermore, an analytical calculation of scaling laws is no longer possible in this case. Nevertheless, it would be worthwhile to pursue such an approach, because it should be possible to clarify some of the problems mentioned above in this way.

The sound attenuation as a function of frequency ω has been measured in Ref. [67] for the system H_2O-octane-$C_{12}E_5$ with 7 wt % amphiphile in the microemulsion phase. For a balanced microemulsion, $\alpha(\omega)\omega^{-2}=D(\omega)c^{-3}(\omega)/2$ is found to be roughly constant for small ω, and to decrease smoothly in the frequency range $1-100$ MHz. This qualitative behavior is in agreement with our theoretical results. It is interesting to note that measurements of sound attenuation and dispersion curves near critical points, where the characteristic frequency ω_c scales as $\omega_c\sim\xi^{-z}$ with the ''dynamic'' exponent $z\simeq 3$ [48,37], are

TABLE II. Correlation propagators.

(a)	$G^{(0)}_{\Phi\Phi}(\mathbf{k},\omega)$	$\dfrac{2\Gamma_\Phi k^m}{\lvert-i\omega+\Gamma_\Phi k^m \chi_0^{-1}(k)\rvert^2}$
(b)	$G^{(0)}_{\rho\rho}(\mathbf{k},\omega)$	$\dfrac{2\Gamma_\rho k^2}{\lvert-i\omega+\Gamma_\rho k^2 \chi_\rho^{-1}(k)\rvert^2}$
(c)	$G^{(0)}_{\mathbf{j}_T\mathbf{j}_T}(\mathbf{k},\omega)$	$\dfrac{2\Gamma_T k^2}{\lvert-i\omega+\Gamma_T k^2\rvert^2}$
(d)	$G^{(0)}_{\mathbf{j}_L\mathbf{j}_L}(\mathbf{k},\omega)$	$\dfrac{2\lambda_0^2\Gamma_p k^4+2\Gamma_L k^2(\omega^2+\Gamma_p^2k^4)}{\lvert\omega^2-\lambda_0^2k^2-\Gamma_L\Gamma_p k^4+i\omega(\Gamma_L+\Gamma_p)k^2\rvert^2}$
(e)	$G^{(0)}_{pp}(\mathbf{k},\omega)$	$\dfrac{2\lambda_0^2\Gamma_L k^4+2\Gamma_p k^2(\omega^2+\Gamma_L^2k^4)}{\lvert\omega^2-\lambda_0^2k^2-\Gamma_L\Gamma_p k^4+i\omega(\Gamma_L+\Gamma_p)k^2\rvert^2}$
(f)	$G^{(0)}_{\mathbf{j}_L p}(\mathbf{k},\omega)$	$\dfrac{2\omega\lambda_0(\Gamma_L+\Gamma_p)k^2\mathbf{k}}{\lvert\omega^2-\lambda_0^2k^2-\Gamma_L\Gamma_p k^4+i\omega(\Gamma_L+\Gamma_p)k^2\rvert^2}$

with $\chi_0^{-1}(k)=2(ck^4+b_0k^2+r_2)$, $\chi_\rho^{-1}(k)=2(\gamma k^4+\beta k^2+\alpha)$

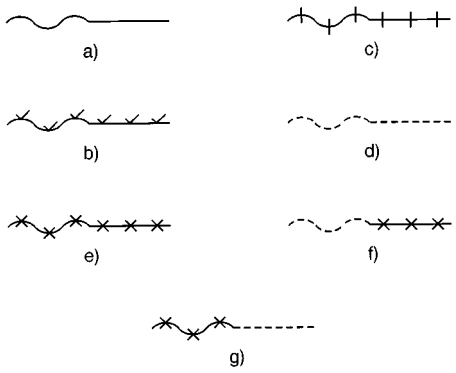

FIG. 17. Bare response functions. Straight lines represent physical fields, wavy lines response fields. Solid lines denote the order parameter propagators, lines with crosses are propagators of the pressure field, lines with check marks represent the amphiphile concentration propagators. For the momentum density **j**, we indicate the longitudinal component $\mathbf{j}_L$ by dashed lines, and the transverse component $\mathbf{j}_T$ by lines with bars. The labels (a)–(g) refer to Table I.

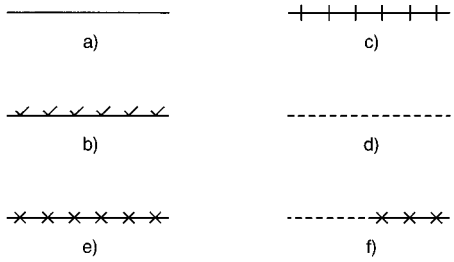

FIG. 18. Bare correlation functions. Straight lines represent physical fields, wavy lines response fields. Solid lines denote the order parameter propagators, lines with crosses are propagators of the pressure field, lines with check marks represent the amphiphile concentration propagators. For the momentum density **j**, we indicate the longitudinal component $\mathbf{j}_L$ by dashed lines, and the transverse component $\mathbf{j}_T$ by lines with bars. The labels (a)–(f) refer to Table II.

usually performed in the same range of frequencies [63,68]. The experiment of Ref. [67] indicates that the sound attenuation has a maximum for a microemulsion near the apex of the three-phase triangle. This is again consistent with our result that the damping $D(\omega)$ should increase with increasing correlation length.

An interesting limit of microemulsion and sponge phases is the case of strongly swollen systems, where the typical domain size of oil and water regions is much larger than the thickness of an amphiphilic mono- or bilayer. In this case, the correlation length ξ, the inverse domain size q, and the ''amphiphile length'' $c^{1/4}$ are given by $\xi\sim\kappa_0\rho_s^{-1}$, $q\sim\rho_s$, and $c^{1/4}\sim\kappa_0^{1/4}\rho_s^{-1/4}$ where κ_0 is the bending rigidity of the amphiphile layer [14]. These relations imply in particular $q\xi\sim\kappa_0$. Although it is unclear whether our results still apply quantitatively in this limit, we believe that the qualitative behavior should be predicted correctly. Thus, we would expect, for example, the zero-shear viscosity to scale as $\eta(0)\sim\kappa_0^2\rho_s^{-2}$. The viscosity of a strongly swollen sponge phase in the system cetylpyridinium chloride-hexanol brine has been investigated experimentally in a *steady-shear* experiment as a function of the shear rate in Ref. [69]. The results show a shear-rate-independent viscosity in the range $0.1-100$ Hz. The zero-shear viscosity is found to increase linearly with the amphiphile concentration ρ_s, in contrast to the theoretical expectation. We believe that the most plausible conceivable explanation for this discrepancy is that steady shear destroys the complex equilibrium structure of a sponge phase already at very small shear rates.

More experimental data are clearly necessary for a detailed test of the theoretical predictions. In particular, it would be interesting to measure simultaneously the static scattering intensity in bulk contrast (to determine q and ξ), the viscosity and the sound attenuation and damping for a series of balanced microemulsions with increasing amphiphile chain length. The correlation length ξ can be varied also by approaching the transition to a spatially ordered

TABLE III. Nondissipative and dissipative vertices.

(a)	$ig_0\mathcal{T}_{q_2}(\mathbf{q}_1+\mathbf{q}_2)=ig_0\mathcal{T}_{q_2}\mathbf{k}$
(b)	$i\tau_0\mathcal{T}_{q_2}(\mathbf{q}_1+\mathbf{q}_2)=i\tau_0\mathcal{T}_{q_2}\mathbf{k}$
(c)	$i\frac{g_0}{2}\mathcal{T}_k[\mathbf{q}_1\chi_0^{-1}(q_1)+\mathbf{q}_2\chi_0^{-1}(q_2)]$
(d)	$i\frac{\tau_0}{2}\mathcal{T}_k[\mathbf{q}_1\chi_\rho^{-1}(q_1)+\mathbf{q}_2\chi_\rho^{-1}(q_2)]$
(e)	$i\tau_0\mathcal{T}_k(\mathbf{q}_2+\mathbf{q}_3)[\beta_1-\frac{1}{2}(2\beta_2+\beta_3)(q_2^2+q_3^2)-2\beta_2\mathbf{q}_2\mathbf{q}_3]$
(f)	$i\frac{g_0}{2}\mathcal{T}_k(\mathbf{q}_1+\mathbf{q}_2+2\mathbf{q}_3)[2\beta_1-(2\beta_2+\beta_3)q_3^2]$
	$-ig_0\beta_3\mathcal{T}_k[(\mathbf{q}_1+\mathbf{q}_3)(q_1^2+\mathbf{q}_1\mathbf{q}_3)+(\mathbf{q}_2+\mathbf{q}_3)(q_2^2+\mathbf{q}_2\mathbf{q}_3)]$
(g)	$\Gamma_\Phi(\mathbf{q}_1+\mathbf{q}_2)^m[2\beta_1-2\beta_3q_1^2-(2\beta_2+\beta_3)q_2^2-2\beta_3\mathbf{q}_1\mathbf{q}_2]$
(h)	$\Gamma_\rho(\mathbf{q}_1+\mathbf{q}_2)^2[\beta_1-\frac{1}{2}(2\beta_2+\beta_3)(q_1^2+q_2^2)-2\beta_2\mathbf{q}_1\mathbf{q}_2]$
with $\chi_0^{-1}(k)=2(ck^4+b_0k^2+r_2)$, $\chi_\rho^{-1}(k)=2(\gamma k^4+\beta k^2+\alpha)$	

phase (if the transition is weakly first order).

Our results for the viscosity, for the sound velocity and damping, and for the dynamic scattering intensity in bulk contrast should also apply to the disordered phase of diblock copolymer melts. In fact, the shear-induced isotropic-to-lamellar transition predicted in Ref. [30], based on a very similar Ginzburg-Landau model, has been confirmed very nicely for a symmetric diblock copolymer melt [70]. Furthermore, the small-ω regime with a quadratic and linear ω dependence of the storage and loss moduli, respectively, has already been observed experimentally in these systems [71,57]. Therefore, it would now be very interesting to determine the characteristic frequency ω^*, and to measure the sound velocity and damping.

ACKNOWLEDGMENTS

We thank J. Goos, D. Kroll, H. Spohn, H. Wagner, and W. Zwerger for many helpful discussions. Conversations with M. Kahlweit, E. Kaler, and S. Ramaswamy are also gratefully acknowledged.

APPENDIX A: RULES FOR FEYNMAN DIAGRAMS

The inversion of the matrix $[G^{(0)}]^{-1}$ — defined in Eqs. (31) to (36) — of the Gaussian action $\mathcal{A}_0$ yields the propagators $G_{ij}^{(0)}(\mathbf{k},\omega)$, which are related to the (unreduced) Gaussian (or van-Hove) response and correlation functions by

$$\langle \Psi_i(\mathbf{k}_1,\omega_1)\Psi_j(\mathbf{k}_2,\omega_2)\rangle_0 = G_{ij}^{(0)}(\mathbf{k}_1,\omega_1)(2\pi)^4\delta(\mathbf{k}_1+\mathbf{k}_2) \times \delta(\omega_1+\omega_2). \tag{A1}$$

The results of this matrix inversion are summarized in Tables I and II; the graphical representations of the propagators are shown in Figs. 17 and 18.

The higher-than-quadratic terms in the dynamic functional $\mathcal{A}$, given by Eq. (25), determine the vertices of the Feynman diagrams, which are listed in Table III, and shown graphically in Fig. 19. It turns out to be convenient to consider the longitudinal and transverse projectors,

$$[\mathcal{L}_k]_{\alpha\beta} \equiv \frac{1}{k^2} k_\alpha k_\beta \tag{A2}$$

and

$$[\mathcal{T}_k]_{\alpha\beta} \equiv \delta_{\alpha\beta} - \frac{1}{k^2} k_\alpha k_\beta \tag{A3}$$

of the momentum density as part of the vertices, and not as part of the propagators. The reason is that in the calculation of self-energy diagrams the external propagators have to be cut off, the corresponding projectors, however, have to be taken into account.

APPENDIX B: FLUCTUATION-DISSIPATION THEOREMS

Fluctuation-dissipation theorems (FDT) provide important relations between the full correlation and response functions.

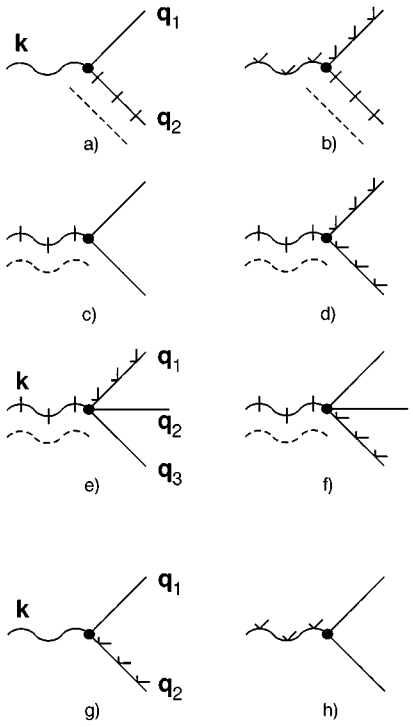

FIG. 19. Dissipative and nondissipative vertices. The labels (a)–(h) refer to Table III.

For an arbitrary dynamic field $\Psi(\mathbf{k},\omega)$, they have the general form [32,72]

$$G_{\Psi\Psi}(\mathbf{k},\omega) = \frac{2}{\omega}\mathrm{Im}\{\Gamma_\Psi(\mathbf{k},\omega)k^n G_{\tilde{\Psi}\Psi}(\mathbf{k},\omega)\}, \tag{B1}$$

where $n=0$ or $n=2$ for nonconserved or conserved fields, respectively. The wave-vector and frequency-dependent dissipative coupling constant (or Onsager coefficient) $\Gamma_\Psi(\mathbf{k},\omega)$ in Eq. (B1) follows from the relation

$$G_{\Psi\Psi}^{(stat)}(\mathbf{k}) = \Gamma_\Psi(\mathbf{k},\omega=0)k^n G_{\tilde{\Psi}\Psi}(\mathbf{k},\omega=0) \tag{B2}$$

between the (full) dynamic response function $G_{\tilde{\Psi}\Psi}(\mathbf{k},t)$ and the (full) static correlation function $G_{\Psi\Psi}^{(stat)}(\mathbf{k})$. Equation (B2) can be derived from Kramers-Kronig relations together with the sum rule

$$G_{\Psi\Psi}^{(stat)}(\mathbf{k}) = \int \frac{d\omega}{2\pi} G_{\Psi\Psi}(\mathbf{k},\omega). \tag{B3}$$

In model H, the static correlation function of the order parameter Φ is given by

$$G_{\Phi\Phi}^{(stat)}(\mathbf{k}) = \chi_0(k) \tag{B4}$$

since we have not taken into account any higher-than-quadratic terms in the static free-energy functional. Therefore, the renormalized Onsager coefficient is found to be

$$\Gamma_\Phi(\mathbf{k},\omega) = \Gamma_\Phi - \frac{\Sigma_{\Phi\tilde{\Phi}}(\mathbf{k},\omega)}{k^m \chi_0^{-1}(k)}, \tag{B5}$$

which implies

$$\Sigma_{\tilde{\Phi}\tilde{\Phi}}(\mathbf{k},\omega) = -2\chi_0(k)\mathrm{Re}\{\Sigma_{\Phi\tilde{\Phi}}(\mathbf{k},\omega)\} \tag{B6}$$

for the self-energy contributions. The same relation applies for the self-energy terms of the amphiphile concentration ρ, if it couples only to the momentum density field. Similarly, one finds

$$\Sigma_{\tilde{\mathbf{j}}_{T,L}\tilde{\mathbf{j}}_{T,L}}(\mathbf{k},\omega) = -2\mathrm{Re}\{\Sigma_{\mathbf{j}_{T,L}\tilde{\mathbf{j}}_{T,L}}(\mathbf{k},\omega)\} \tag{B7}$$

for the momentum density field.

In model C, a one-loop calculation shows that

$$\Sigma_{\rho\tilde{\rho}}(\mathbf{k},\omega=0) = \Gamma_\rho k^2 \Sigma_\rho^{(stat)}(\mathbf{k}) \tag{B8}$$

which yields the relation

$$G_{\rho\rho}^{(stat)}(\mathbf{k}) = \frac{1}{\chi_0^{-1}(k) - \Sigma_\rho^{(stat)}(\mathbf{k})} = \Gamma_\rho k^2 G_{\tilde{\rho}\rho}(\mathbf{k},\omega=0). \tag{B9}$$

The condition (B2) then implies that the Onsager coefficient of the amphiphile concentration remains unrenormalized in this case,

$$\Gamma_\rho(\mathbf{k},\omega) = \Gamma_\rho. \tag{B10}$$

Therefore, the relation between the self-energy terms reads

$$\Sigma_{\tilde{\rho}\tilde{\rho}}(\mathbf{k},\omega) = \frac{2\Gamma_\rho k^2}{\omega}\mathrm{Im}\{\Sigma_{\rho\tilde{\rho}}(\mathbf{k},\omega)\}. \tag{B11}$$

Equations (B6), (B7), and (B11) have been used in this paper to calculate the self-energy contributions $\Sigma_{\tilde{\Psi}\tilde{\Psi}}$ in a simple way. It is also possible, of course, to calculate these self-energy terms directly from the corresponding Feynman diagrams. Since the FDT relations have to be satisfied in any order of a loop expansion, they can be used as a test of a correct and consistent calculation of the Feynman diagrams in this case.

[1] J. Meunier, D. Langevin, and N. Boccara, *Physics of Amphiphilic Layers* (Springer, Berlin, 1987).

[2] G. Gompper and M. Schick, in *Phase Transitions and Critical Phenomena*, edited by C. Domb and J. Lebowitz (Academic, London, 1994), Vol. 16, pp. 1–176.

[3] *Micelles, Membranes, Microemulsions, and Monolayers*, edited by W. Gelbart, D. Roux, and A. Ben-Shaul (Springer, Berlin, 1995).

[4] M. Teubner and R. Strey, J. Chem. Phys. **87**, 3195 (1987).

[5] C. Vonk, J. Billman, and E. Kaler, J. Chem. Phys. **88**, 3970 (1988).

[6] S.-H. Chen, S.-L. Chang, and R. Strey, J. Chem. Phys. **93**, 1907 (1990).

[7] B. Lindman *et al.*, Colloids Surf. **38**, 205 (1989).

[8] W. Jahn and R. Strey, J. Phys. Chem. **92**, 2294 (1988).

[9] G. Porte, J. Phys. Condens. Matter **4**, 8649 (1992).

[10] D. Roux, C. Coulon, and M. Cates, J. Phys. Chem. **96**, 4174 (1992).

[11] B. Widom, J. Chem. Phys. **90**, 2437 (1989).

[12] G. Gompper and M. Schick, Phys. Rev. B **41**, 9148 (1990).

[13] M. Skaf and G. Stell, J. Chem. Phys. **97**, 7699 (1992).

[14] P. Pieruschka and S. Safran, Europhys. Lett. **22**, 625 (1993).

[15] D. Roux *et al.*, Europhys. Lett. **11**, 229 (1990).

[16] G. Gompper and M. Schick, Phys. Rev. E **49**, 1478 (1994).

[17] G. Gompper and J. Goos, Phys. Rev. E **50**, 1325 (1994).

[18] G. Gompper and U. Schwarz, Z. Phys. B **97**, 233 (1995).

[19] P. Pieruschka, S. Safran, and S. Marčelja, Phys. Rev. E **52**, 1245 (1995).

[20] G. Gompper and J. Goos, Phys. Rev. E **52**, 1248 (1995).

[21] M. Skouri, J. Marignan, J. Appell, and G. Porte, J. Phys. (France) II **1**, 1121 (1991).

[22] M. Filali, G. Porte, J. Appell, and P. Pfeuty, J. Phys. (France) II **4**, 349 (1994).

[23] C. Vinches, C. Coulon, and D. Roux, J. Phys. (France) II **4**, 1165 (1994).

[24] G. Gompper and M. Hennes, Phys. Rev. Lett. **73**, 1114 (1994).

[25] G. Gompper and M. Hennes, J. Phys. (France) II **4**, 1375 (1994).

[26] R. Granek, M. E. Cates, and S. Ramaswamy, Europhys. Lett. **19**, 499 (1992).

[27] R. Granek and M. E. Cates, Phys. Rev. A **46**, 3319 (1992).

[28] C. Mundy, Y. Levin, and K. Dawson, J. Chem. Phys. **97**, 7695 (1992).

[29] G. Gompper and M. Hennes, Europhys. Lett. **25**, 193 (1994).

[30] M. E. Cates and S. T. Milner, Phys. Rev. Lett. **62**, 1856 (1989).

[31] R. Graham, in *Quantum Statistics in Optics and Solid-State Physics*, Springer Tracts in Modern Physics Vol. 66, edited by G. Höhler and E. Niekisch (Springer, Berlin, 1973).

[32] U. Deker and F. Haake, Phys. Rev. A **11**, 2043 (1975).

[33] S. Ma and G. Mazenko, Phys. Rev. B **11**, 4077 (1975).

[34] C. De Dominicis and L. Peliti, Phys. Rev. B **18**, 353 (1978).

[35] P. Hohenberg and B. Halperin, Rev. Mod. Phys. **49**, 435 (1977).

[36] M. Nolan, Phys. Rev. B **18**, 6334 (1978).

[37] D. M. Kroll and J. M. Ruhland, Phys. Rev. A **23**, 371 (1981).

[38] G. Gompper and M. Schick, Phys. Rev. Lett. **65**, 1116 (1990).

[39] G. Gompper, R. Hołyst, and M. Schick, Phys. Rev. A **43**, 3157 (1991).

[40] J. Putz, R. Hołyst, and M. Schick, Phys. Rev. A **46**, 3369 (1992).

[41] G. Gompper and M. Hennes, J. Chem. Phys. **102**, 2871 (1995).

[42] F. Schmid and M. Schick, J. Chem. Phys. **102**, 7197 (1995).

[43] In Ref. [29], an additional $p\Phi^2$ term has been included in the free-energy functional $\mathcal{F}_{HD}$. Such a term was found to be important in the calculation of the sound attenuation and dispersion of one-component liquids near a liquid-gas critical point in Ref. [73]. On the other hand, such a term plays no role near the demixing transition of binary fluids [37]. Thus we conclude that although such a term cannot be excluded from symmetry arguments, it is not important for ternary amphiphilic systems; this is indeed borne out by a more detailed analysis. Thus its contribution is neglected here.

[44] R. Graham and H. Haken, Z. Phys. **243**, 289 (1971).

[45] P. C. Martin, O. Parodi, and P. S. Pershan, Phys. Rev. A **6**, 2401 (1972).

[46] L. Kadanoff and P. Martin, Ann. Phys. (N.Y.) **24**, 419 (1963).
[47] D. Forster, *Hydrodynamic Fluctuations, Broken Symmetry, and Correlation Functions* (Benjamin/Cummings, London, 1975).
[48] K. Kawasaki, in *Phase Transitions and Critical Phenomena*, edited by C. Domb and M. Green (Academic, London, 1976), Vol. 5a.
[49] E. Siggia, B. Halperin, and P. Hohenberg, Phys. Rev. B **13**, 2110 (1976).
[50] B. Halperin, P. Hohenberg, and S. Ma, Phys. Rev. B **10**, 139 (1974).
[51] P. C. Martin, E. D. Siggia, and H. A. Rose, Phys. Rev. A **8**, 423 (1973).
[52] R. Bausch, H. K. Janssen, and H. Wagner, Z. Phys. B **24**, 113 (1976).
[53] The same expressions for the sound velocity and damping have been derived for a Ginzburg-Landau model of the critical behavior of ^{4}He in Refs. [74,75].
[54] T. S. Chow, Phys. Rev. E **50**, 1274 (1994).
[55] J. van der Werff, C. de Kruif, C. Blom, and J. Mellema, Phys. Rev. A **39**, 795 (1989).
[56] The exact agreement of the zero shear viscosity Eq. (58) with the result of Ref. [28] may be fortuitious, since the expressions for the frequency dependence of the viscosity are different in the two approaches.
[57] G. H. Fredrickson and R. G. Larson, J. Chem. Phys. **86**, 1553 (1987).
[58] B. Cichocki and B. U. Felderhof, Phys. Rev. A **43**, 5405 (1991).
[59] R. G. Larson and G. L. Fredrickson, Macromolecules **20**, 1897 (1987).
[60] T. Ohta and K. Kawasaki, Macromolecules **19**, 2621 (1986).
[61] G. H. Fredrickson and E. Helfand, J. Chem. Phys. **87**, 697 (1987).
[62] J. D. Ferry, *Viscoelastic Properties of Polymers* (Wiley, New York, 1980).
[63] J. Thoen and C. Garland, Phys. Rev. A **10**, 1311 (1974).
[64] We want to mention parenthetically that for the sound modes a complex longitudinal modulus $M(\omega)$ can be defined [76] in analogy to the storage and loss modulus of the viscosity. Our results show that not the longitudinal modulus itself, but $[M(\omega)-M(0)]/\omega$ has a scaling form and should thus be considered.
[65] The small-frequency behavior of the sound dispersion was found numerically in Ref. [29] to be described by $\Delta(\omega)\sim\omega^2$. This result represents only a rough estimate; the correct asymptotic behavior is given by $\Delta(\omega)\sim\omega^{3/2}$.
[66] C. M. Bender and S. A. Orszag, *Advanced Mathematical Methods for Scientists and Engineers* (McGraw-Hill, New York, 1978).
[67] M. Kahlweit *et al.*, J. Colloid Interface Sci. **118**, 436 (1987).
[68] F. Vidal, J. Tarvin, and T. Greytak, Phys. Rev. B **25**, 7040 (1982).
[69] P. Snabre and G. Porte, Europhys. Lett. **13**, 641 (1990).
[70] K. Koppi, M. Tirrell, and F. S. Bates, Phys. Rev. Lett. **70**, 1449 (1993).
[71] F. S. Bates, Macromolecules **17**, 2607 (1984).
[72] H.-K. Janssen, in *Dynamical Critical Phenomena and Related Topics*, edited by C. Enz (Springer, Berlin, 1979).
[73] D. M. Kroll and J. M. Ruhland, Phys. Lett. A **80**, 45 (1980).
[74] J. Pankert and V. Dohm, Europhys. Lett. **2**, 775 (1986).
[75] J. Pankert and V. Dohm, Phys. Rev. B **40**, 10856 (1989).
[76] K. Herzfeld and T. Litovitz, *Absorption and Dispersion of Ultrasonic Waves* (Academic, New York, 1959).